Theory of phonon dispersion relations in semiconductor superlattices

Sung-kit Yip and Yia-Chung Chang
Department of Physics and Materials Research Laboratory, University of Illinois at Urbana-Champaign, Urbana, Illinois 61801
(Received 7 May 1984)

In this paper we study the phonon dispersion in superlattices consisting of alternating layers of semiconductors. First the parameters in the adiabatic bond-charge model are obtained. Then it is shown that an excellent approximation to the dispersion curves of the bulk semiconductors can be obtained first by a zeroth-order calculation which includes only short-range forces and Coulomb interactions between ions and bond charges in the same and neighboring layers, then by a first-order perturbation to include the effect of the remaining forces. Thus it is possible to obtain the complex phonon dispersion relations via the eigenvalue method in the zeroth-order calculation. The eigenmode displacements of the superlattice are obtained by matching the eigenvectors associated with complex phonon branches at the interfaces, and the superlattice phonon dispersion curves including the effect of interlayer Coulomb interactions are calculated in the first-order approximation. The results for the superlattice phonon frequencies compare very favorably with the existing experimental data.

I. INTRODUCTION

With modern technologies, superlattices made up of alternating layers of semiconductors have been fabricated in the laboratory. Considerable effort has been spent to understand their electronic properties.[1] However, only very little work has been done on their phonon properties. The problem was first considered by Rytov[2] in a continuum model. Later, Barker *et al.*[3] took the lattice into account by using a simple linear-chain model with short-range forces to calculate the phonon dispersion curves of the AlAs/GaAs(001) superlattice. However, as pointed out by Merlin *et al.*,[4] the long-range Coulomb interaction cannot be neglected in obtaining the dispersion curves. In this paper we shall present a method which takes both the presence of a lattice and the long-range Coulomb interaction into account.

We first adopt a model for the phonon calculation of bulk semiconductors. Once this is done, we may try to solve the superlattice problem in a straightforward manner with use of the force constants of the known model by writing the equations of motions for the ions of the superlattice, and then solving for the frequencies in the same way as for a bulk material.[5] However, this method, though simple, has the drawback that the size of the matrices increases linearly with the superlattice unit-cell length. The calculation soon becomes difficult and even numerically intractable.

The similarity of a phonon-dispersion-relation calculation with the electronic band-structure calculation in the tight-binding approximation suggests that we may try to solve the problem using the idea of complex band structure.[6,7] However, finding the complex phonon dispersion relations[1] of a realistic phonon model is not a trivial task because of the existence of the long-range Coulomb interaction.

In this paper we shall show that we can treat the problem by a perturbation method, using a zeroth-order model, in which the Coulomb interaction between any two layers of ions is truncated at a short distance, and with the remaining Coulomb interaction treated as a perturbation. We find that the dispersion curves for the bulk obtained in this way are extremely close to those obtained by a full calculation. With this, we can proceed in a way analogous to the electronic "complex band-structure" calculation[8] to obtain the complex phonon dispersion and the associated eigenvectors in the zeroth-order approximation, then match them at the boundaries, and finally reinstate the remaining long-range Coulomb interaction using a first-order perturbation theory. This is the procedure that we shall follow.

In Sec. II we first review the adiabatic bond-charge model,[9–11] which we adopt for describing the lattice dynamics. Then, a justification for our approach of treating the long-range part of the Coulomb interaction as a perturbation is presented. In Sec. III we calculate the complex phonon dispersion relations in the zeroth-order approximation and discuss the results. In Sec. IV the complex phonon dispersion relations are used to calculate the phonon dispersion relations for the AlAs/GaAs(001) superlattice for a particular case in which the wave vector is in the z direction. Section V constitutes a summary of our results.

II. REVIEW OF THE ADIABATIC BOND-CHARGE MODEL FOR III-V—COMPOUND SEMICONDUCTORS

We shall adopt the adiabatic bond-charge model[9–11] (BCM) for the description of the lattice dynamics which is an extension of Martin's simple bond-charge model.[12] We shall not dwell on the merit of the BCM over the more conventional shell model for semiconductors[13] since the reasons have been discussed in detail in the original works.[10,11] We shall just give a brief review of the model itself for convenience of later reference and establishment

of notation.

Martin[12] showed that in III-V—compound semiconductors there are two kinds of bonding forces: metal-like and covalent. In the BCM the former is represented by a nearest-neighbor interaction potential $\phi_{i\text{-}i}$ between the ions, while the latter is represented by interactions involving the bond charges (BC's), whose positions divide the bond length between the cation and the anion (hereafter referred to as $\kappa=1$ and 2, respectively) in the ratio 5:3. Thus if t_0 is the bond length, then the two ion—bond-charge distances are $r_1=t_0(1+p)/2$ and $r_2=t_0(1-p)/2$, respectively, where $p=0.25$. The charges of the ions are $Z_1=Z_2=2Z$, and that of the BC's is $-Z$ (see Fig. 1). In the adiabatic BCM, the BC's are allowed to move adiabatically.[9-11]

We shall denote the two ion—bond-charge potentials by ϕ_1 and ϕ_2. Any two BC's i,j, centered around a common ion σ, interact with each other and with the ion via a Keating potential,[14]

$$V_{bb}^{(\sigma)}=\tfrac{1}{2}B_\sigma(\vec{X}_{\sigma i}\cdot\vec{X}_{\sigma j}+a_0^2)^2/4a_\sigma^2 ,$$

where $\vec{X}_{\sigma i},\vec{X}_{\sigma j}$ are the distance vectors at any given instance between ion σ ($\sigma=1,2$) and bond charges i,j, B_σ are force constants, and a_σ^2 is the equilibrium value of $|\vec{X}_{\sigma i}\cdot\vec{X}_{\sigma j}|$, i.e., $a_1^2=\frac{1}{3}[t_0(1+p)/2]^2$ and $a_2^2=\frac{1}{3}[t_0(1-p)/2]^2$. The BC's also interact directly with each other via a potential ψ_1 or ψ_2, depending on whether they are centered around ion 1 or 2. We shall follow Rustagi and Weber[10] and assume that $\psi_1'=\psi_2'=0$ and $\psi_1''=-\psi_2''\equiv(B_2-B_1)/8$. Here, and henceforth, all derivatives are evaluated at the equilibrium distance between the ions or BC concerned.

We write the Coulomb interaction energy per unit cell as

$$-\alpha_M\frac{(2Z)^2}{\epsilon}\frac{e^2}{t_0} ,$$

where ϵ is the dielectric constant and α_M is the Madelung constant for the model. The equilibrium conditions for the minimization of the total energy per unit cell (Φ) with respect to t_0 and p are given by

$$0=\left.\frac{\partial\Phi}{\partial t}\right|_{t=t_0}=\left.\frac{\partial\Phi}{\partial p}\right|_{p=0.25} , \tag{1}$$

where

$$\Phi=4\phi_1(r_1)+4\phi_2(r_2)+4\phi_{i\text{-}i}(t_0)-\alpha_M\frac{(2Z)^2e^2}{\epsilon t_0}+6[V_{bb}^{(1)}+V_{bb}^{(2)}]+6\left[\psi_1\left[\frac{1+p}{2}\frac{4t_0}{\sqrt{6}}\right]+\psi_2\left[\frac{1-p}{2}\frac{4t_0}{\sqrt{6}}\right]\right] .$$

From (1) we obtain

$$\phi_{i\text{-}i}'=-\frac{\alpha_M Z^2}{2\epsilon t_0^2}$$

and

$$\phi_1'-\phi_2'=2\frac{d\alpha_M}{dp}\frac{Z^2}{\epsilon}\frac{e^2}{t_0^2} . \tag{2}$$

Following Rustagi and Weber,[10] we take the additional assumption that $(1+p)\phi_1'+(1-p)\phi_2'=0$, and obtain

$$\frac{\phi_1'}{r_1}=2\frac{1-p}{1+p}\frac{d\alpha_M}{dp}\frac{Z^2}{\epsilon}\frac{1}{t_0^3} , \tag{3}$$

$$\frac{\phi_2'}{r_2}=2\frac{1+p}{1-p}\frac{d\alpha_M}{dp}\frac{Z^2}{\epsilon t_0^3} . \tag{4}$$

At $p=0.25$, α_M and $d\alpha_M/dp$ are numerically determined to be 4.779 and 2.764, respectively. Hence, the (independent) parameters of the model are $\phi_{i\text{-}i}''$, ϕ_1'', ϕ_2'', B_1, B_2, and Z^2/ϵ. Together with (2)—(4), and ψ_1'' and ψ_2'', we can write the force-constant matrices between the ions and BC's as shown in Appendix A. The dynamical matrix[5] is then

$$D_{\alpha\beta}\begin{bmatrix}\vec{k}\\ \kappa\ \ \kappa'\end{bmatrix}=\sum_{l'}\Phi_{\alpha\beta}(l,\kappa;l',\kappa')e^{-i\vec{k}\cdot[\vec{x}(l)-\vec{x}(l')]} , \tag{5}$$

where $\vec{x}(l)\equiv\vec{x}(l,1)$ is the lattice vector in the lth unit cell,

$$\Phi_{\alpha\beta}(l,\kappa;l',\kappa')\equiv\frac{\partial\Phi}{\partial X_{l\kappa,\alpha}\partial X_{l'\kappa',\beta}} ,$$

$X_{l\kappa,\alpha}$ is the αth component of the position vector of the ion κ or BC κ in unit cell l, and $\vec{k}$ is the wave vector. The equation of motion is then

$$M_\kappa\omega^2u_\alpha(l,\kappa)=\sum_{l',\kappa',\beta}\Phi_{\alpha\beta}(l,\kappa;l',\kappa')u_\beta(l',\kappa') . \tag{6}$$

With the displacement $u_\alpha(l,k)$ of the ion κ in unit cell l associated with the jth mode written as

$$u_\alpha(l,\kappa)=e^{i\vec{k}\cdot\vec{x}(l)}\epsilon_\alpha(\kappa\,|\,\vec{k},j) , \tag{7}$$

and using definition (5), we can rewrite (6) as

$$M_\kappa\omega^2\epsilon_\alpha(\kappa\,|\,\vec{k},j)=\sum_{\kappa',\beta}D_{\alpha\beta}\begin{bmatrix}\vec{k}\\ \kappa\ \ \kappa'\end{bmatrix}\epsilon_\beta(\kappa'\,|\,\vec{k},j) , \tag{8}$$

from which $\omega^2(\vec{k})$ can be obtained by diagonalization.[9,11]

Table I shows the parameters of the model for seven III-V—compound semiconductors. The parameters for GaP, GaAs, GaSb, and InSb are adopted from Ref. 10. The InP parameters are obtained by fitting to the known frequencies at the Γ, X, and L points of the Brillouin zone. The results, accompanied with the data from Refs. 15—17, are shown in Fig. 2. The agreement is very good.

For the other III-V compounds, in particular AlAs, which is of interest here, the available experimental data are too scarce to allow the previous procedure. However, we observe that there is a discernible trend of the parame-

TABLE I BCM parameters for some III-V—compound semiconductors, given in units of e^2/v_a, where v_a is the unit-cell volume.

	Ion-ion	Ion—bond-charge		bond-charge—ion—bond-charge		
	$\frac{1}{3}\phi''_{i\text{-}i}$	$\frac{1}{3}\phi''_1$	$\frac{1}{3}\phi''_2$	B_1	B_2	Z^2/ϵ
AlAs[a]	5.80	2.27	15.48	5.79	8.54	0.180
GaP[b]	6.04	2.40	17.91	5.2	10.0	0.203
GaAs[b]	6.16	2.36	16.05	5.36	8.24	0.187
GaSb[b]	6.77	2.37	13.10	6.28	7.08	0.160
InP[c]	7.16	2.95	21.62	3.43	8.37	0.249
InAs[d]	7.31	2.64	17.86	3.99	7.30	0.210
InSb[b]	7.47	2.32	14.09	4.56	6.24	0.172

[a]Parameters for AlAs are interpolated from the GaAs and (interpolated) InAs values, from Eq. (10), for which the value $y=0.76$ is obtained by fitting the Γ-point frequencies and acoustic frequencies at point X (Ref. 20).
[b]Parameters for GaP, GaAs, GaSb, and InSb are adopted from Rustagi and Weber (Ref. 10).
[c]Parameters for InP are obtained by fitting to the known frequency at points Γ, X, and L.
[d]Parameters for InAs are interpolated from the InP and InSb values, from Eq. (9b).

ters as we move vertically down the Periodic Table and, in fact, we find, to a good approximation,

$$P_{\mathrm{GaAs}}=\tfrac{1}{2}(P_{\mathrm{GaP}}+P_{\mathrm{GaSb}})\ , \tag{9a}$$

where P_S denotes any one of the six BCM parameters listed in Table I, for semiconductor compound S. We believe that the same (approximate) relation holds with substitution of Ga by In in Eq. (9a), and thus we have obtained the corresponding parameters of InAs listed in Table I, by using

$$P_{\mathrm{InAs}}=\tfrac{1}{2}(P_{\mathrm{InP}}+P_{\mathrm{InSb}})\ . \tag{9b}$$

The phonon dispersion curves of InAs calculated in the $[\zeta 00]$, $[\zeta\zeta 0]$, and $[\zeta\zeta\zeta]$ directions are shown in Fig. 3, together with data at Γ from Ref. 18 (see also Ref. 19). We see that the calculated frequencies are very close to the experimental data, despite the fact that (9) may seem rather naive.

We may well suppose a similar equation for the relations between the parameters of semiconductors of the same anion but different cation constituents. We propose that, for some y between 0 and 1,

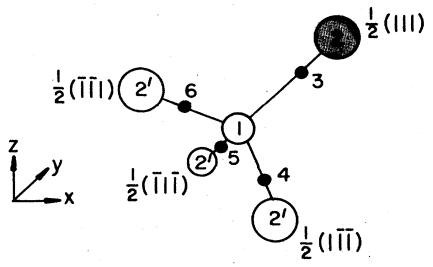

FIG. 1. Unit cell of a III-V—compound semiconductor in the BCM. It consists of cation 1, anion 2, and BC's 3, 4, 5, and 6. Anions of three neighboring unit cells, labeled 2', are also shown, with position vectors relative to the cation given in units of $a/2$, where a is the lattice constant of the conventional (cubic) cell.

$$P_{\mathrm{AlAs}}=\frac{1}{y}P_{\mathrm{GaAs}}-\frac{1-y}{y}P_{\mathrm{InAs}}\ . \tag{10}$$

We obtain y by varying it to fit the Γ-point frequencies and acoustic frequencies at the X point.[20] (In Ref. 20 the optical frequencies at X are also available, but we do not use them in our fitting for reasons which shall be mentioned below.) We obtain $y=0.76$ and thus the parameters for AlAs listed in Table I with use of Eq. (10). The calculated phonon dispersion curves in the $[\zeta 00]$, $[\zeta\zeta 0]$, and $[\zeta\zeta\zeta]$ directions are shown in Fig. 4. There is good agreement between the calculated frequencies and the experimental data, except for one optical frequency at point X. We have, in fact, tried to fit the six parameters of the model to the six known frequencies. We are unable to obtain a good fit within the domain where the parameters

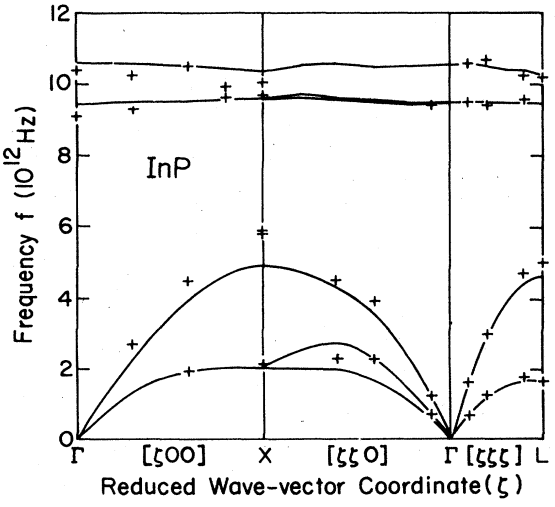

FIG. 2. InP phonon dispersion curves calculated by the BCM. Experimental data (marked +) from Refs. 15—17 are included for comparison.

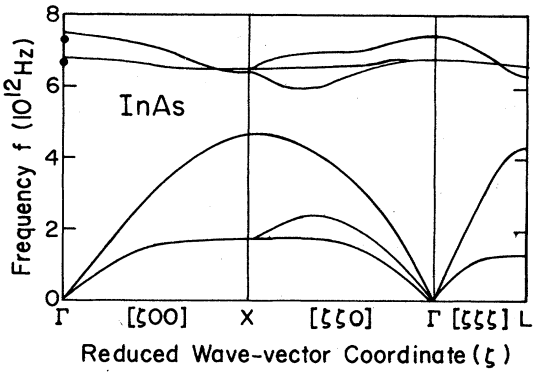

FIG. 3. InAs phonon dispersion curves calculated by the BCM. Experimental data (marked ●) from Ref. 18 are included for comparison.

are physically reasonable. In fact, there is also confusion about which of the two optical frequencies at point X is transverse or longitudinal (see Ref. 3). The optical-frequency data at point X of Ref. 20 is thus in doubt.

It was shown by Weber[11] that, for the group-IV elemental semiconductors, a model with only some short-range part of the Coulomb force included can also fit the experimental data quite well. We shall now investigate a similar question for the III-V—compound semiconductors. We shall only include the Coulomb interaction between an ion and its nearest BC's, and also among BC's which surround a common anion or cation, ignoring all the rest. This can be done with the replacement

$$\phi_1''\rightarrow\phi_1''-\left[\frac{2Z^2}{\epsilon r_1}\right]'',$$

$$\psi_{1,2}''\rightarrow\psi_{1,2}''+\left[\frac{Z^2}{\epsilon\{(4t_0/\sqrt{6})[(1\pm p)/2]\}}\right]'',$$

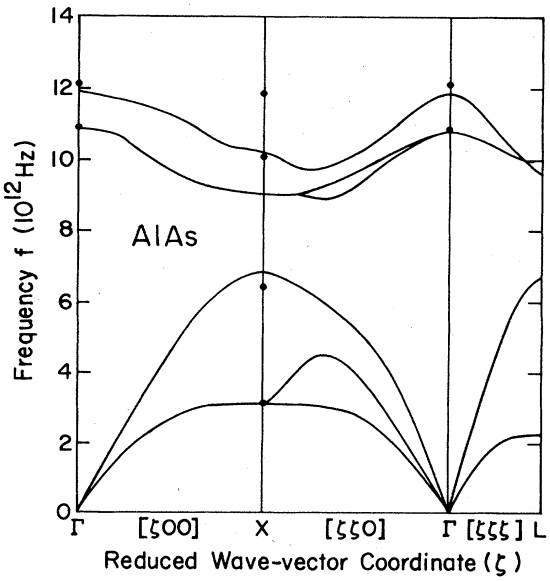

FIG. 4. AlAs phonon dispersion curves calculated by the BCM. Experimental data (marked ●) from Ref. 20 are included for comparison.

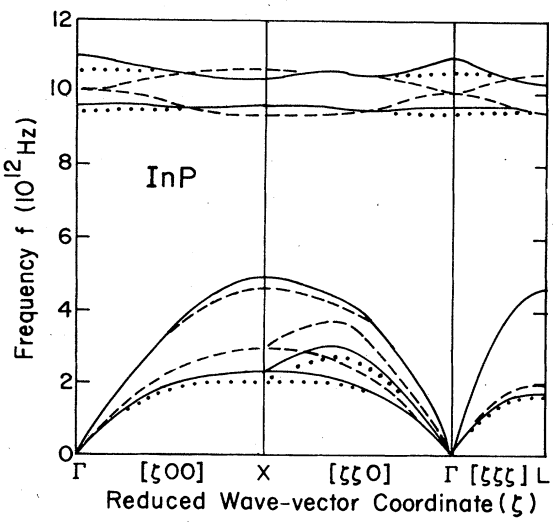

FIG. 5. InP phonon dispersion curves calculated in various stages: the zeroth-order approximation (dashed lines), the first-order approximation (solid lines), and the full calculation in the BCM (dotted lines).

and with all of the Coulomb interaction ignored. For the first derivatives of the potential, we shall choose the new values such that the equations corresponding to (1) are satisfied. The necessary replacement is found to be $\alpha_M\rightarrow 4.614$ and $d\sigma_M/dp\rightarrow 2.461$. This ensures the stability of our model so that the frequencies obtained are real. The result for InP is shown in Fig. 5. We do not obtain good agreement, as expected, because the crystal is heteropolar. Polarization, and hence electric field, is set up due to the relative displacement between the ions and BC's when the lattice vibrates. In particular, due to the absence of this long-range macroscopic electric field, the optical frequencies at point Γ become degenerate.

To see how the results can be improved, we break down the full dynamical matrix into two terms,

$$D_{\alpha\beta}\begin{bmatrix}\vec{k}\\ \kappa\ \kappa'\end{bmatrix}=D^{(0)}_{\alpha\beta}\begin{bmatrix}\vec{k}\\ \kappa\ \kappa'\end{bmatrix}+\delta D^{(1)}_{\alpha\beta}\begin{bmatrix}\vec{k}\\ \kappa\ \kappa'\end{bmatrix}.$$

The first term is the dynamical matrix of the short-range force-constant model just mentioned, and the second term includes the remaining corrections (both the long-range Coulomb terms, the change in the short-range forces mentioned in the last paragraph, and changes necessary due to translational invariance[5]). We now try to treat the second term as a perturbation. With the unperturbed solution chosen to have the orthogonal property (with respect to the semidefinite matrix of the masses M_κ), i.e.,

$$\sum_{\kappa,\alpha} M_\kappa[\epsilon^{(0)}_\alpha(\kappa\mid\vec{k},j')]^*\epsilon^{(0)}_\alpha(\kappa\mid\vec{k},j)=\delta_{jj'}, \tag{11}$$

where (0) denotes the unperturbed solution. We can show by perturbation theory that, to first order,

$$(\omega_j^{(1)})^2=(\omega_j^{(0)})^2+\sum_{\kappa,\alpha}\sum_{\kappa',\beta}[\epsilon_\alpha^{(0)}(\kappa\,|\,j)]^*(D^{(1)})_{\alpha\beta}\begin{bmatrix}\vec{k}\\ \kappa\ \ \kappa'\end{bmatrix}\epsilon_\beta^{(0)}(\kappa'\,|\,j')\ . \tag{12}$$

Although the zeroth-order solution is degenerate at point Γ, no degenerate perturbation theory is needed since the displacement there can be separated into a longitudinal and two orthogonal transverse modes. The result of the calculation is also shown in Fig. 5. The result agrees quite well with the curve of the full calculation.

We see that the long-range part of Coulomb forces in the BCM cannot be neglected, but can be treated as a perturbation, and a first-order perturbation theory is good enough for most purposes. In the next section we will show that by including the intraplane Coulomb interaction in the zeroth-order dynamic matrix and treating the remaining long-range interaction as the perturbation, we can obtain a phonon dispersion relation in nearly perfect agreement with the full calculation.

III. COMPLEX PHONON DISPERSION RELATIONS

A. Method

In the preceding section we showed that we can calculate the dispersion curves first with short-range terms only, and then perform a perturbation. Thus we can use the eigenvalue method[8] to obtain the complex phonon dispersion relations in the zeroth-order approximation. However, for the purpose of studying phonon dispersion relations of heterostructures, we try to avoid the degeneracy of the optical-mode frequencies at the Γ point for the unperturbed solution encountered in the preceding section. To do this we imagine that our bulk material is anisotropic, with the z direction (the direction perpendicular to the interface in a heterostructure of interest) as the special direction. In this paper we shall confine ourselves to the [001] case, although the method is readily applicable for other directions as well. Now, we include in our zeroth-order calculation the Coulomb interaction between (1) an ion layer and its two nearest BC layers, (2) any two neighboring BC layers, (3) any two BC's in the same layer, and (4) any two ions in the same layer. This is illustrated in Fig. 6.

As in Sec. II, we use the parameters in Table I, while modifying the first derivatives of the potentials so that the crystal has a minimum energy. This is discussed in detail in Appendix B. The result is that in (2)—(4) we only have to make the replacement $\alpha_M \rightarrow 5.326$ with $d\alpha_M/dp$ unchanged. For the Coulomb interaction, a sum over all ions or BC's in a layer is needed. This is done in Appendix C.

To illustrate the suitability of this model for calculating heterostructure phonon properties, we first calculate the phonon dispersion relation of a bulk material in first-order perturbation theory, analogous to what we did in Sec. II. Figure 7 shows the unperturbed and perturbed

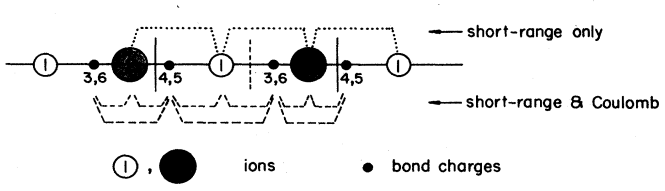

FIG. 6. Schematic diagram of the coupling between layers of ions and BC's due to the short-range and Coulomb interactions included in the zeroth-order model. The dotted lines at top denote the couplings due to short-range interactions only, and the dashed lines at bottom denote the couplings due to both short-range and Coulomb interactions.

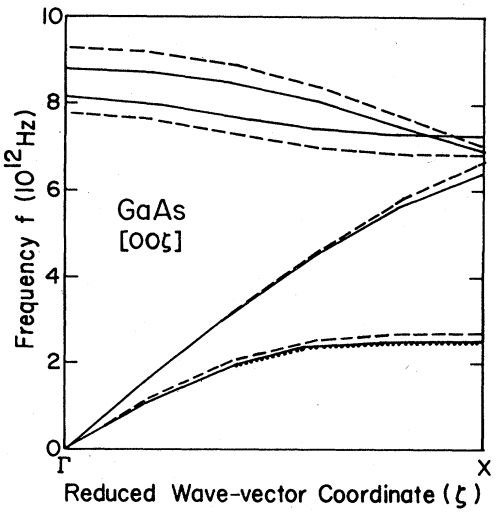

FIG. 7. Phonon dispersion relation of (a) GaAs and (b) AlAs along the [00ζ] direction calculated in three stages: the zeroth-order approximation (dashed lines), the first-order approximation (solid lines), and the full calculation in the BCM (dotted lines).

frequencies for GaAs and AlAs along the $[00\zeta]$ direction and the result of the full calculation. We see that the perturbation itself is small. Therefore, the first-order-perturbed frequencies and those of a full solution agree almost perfectly, except for a very slight discrepancy for the transverse-acoustic branch (the rest agree so well that we cannot even show the difference in the figure). For other directions, we find similar agreement, although not as perfect. As an example, in Fig. 8 we plot the unperturbed and perturbed frequencies for GaAs along the $[\zeta 00]$ direction and the results of the full calculation. Because of the anisotropy introduced in the model, the transverse modes that are degenerate in the full calculation now split into two branches, and the unperturbed frequencies are quite different from those in Fig. 7(a). The perturbed frequencies, however, are still very close to those obtained in the full calculation. The success of this first-order perturbation theory shows that the displacement vectors are sufficiently accurate. This is important since they will be used in our calculation of the superlattice phonon modes when we match the displacements on the boundaries between two materials. In addition, we see that a higher-order perturbation theory is not necessary.

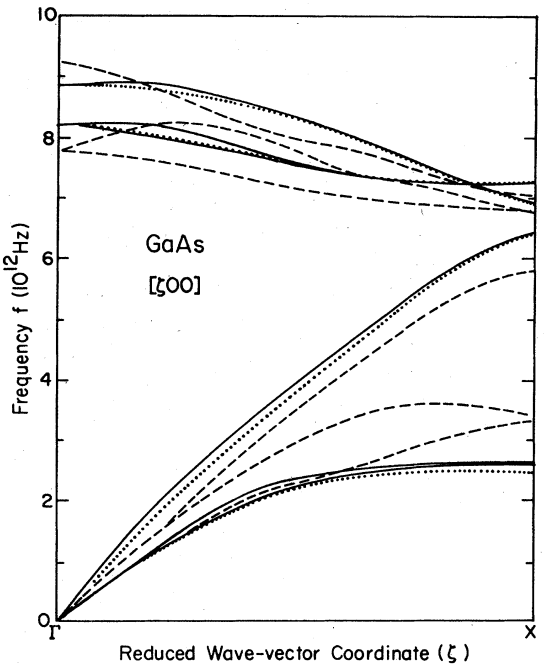

FIG. 8. Phonon dispersion relation of GaAs, along the $[\zeta 00]$ direction, calculated in three stages: the zeroth-order approximation (dashed lines), the first-order approximation (solid lines), and the full calculation in the BCM (dotted lines).

We can now apply the eigenvalue method[8] to find the complex phonon dispersion relation. We write the displacement of the κth ion or BC as (dropping the $\vec{k},j$ indices in the eigenvector)

$$u_\alpha(l,\kappa)=\epsilon_\alpha(\kappa)e^{i(k_z l_3)\pi}e^{i\vec{k}_{||}\cdot\vec{R}_{||}\pi}, \tag{13}$$

where l_3 denotes the layer position; $\vec{k}_{||},\vec{R}_{||}$ are the wave vector and unit-cell position vector, respectively, projected in the x-y plane. (Here, and henceforth, all distances are measured in $a/2$ and wave numbers in $2\pi/a$, where a is the lattice constant.)

Transposing the mass terms to the right-hand side in the equation of motion (8), we obtain

$$0=\sum_{\kappa',\beta} H_{\alpha\beta}\begin{bmatrix} k_z,\vec{k}_{||} \\ \kappa\ \ \kappa' \end{bmatrix}\epsilon_\beta(\kappa'), \tag{14}$$

where

$$H_{\alpha\beta}\begin{bmatrix} k_z,\vec{k}_{||} \\ \kappa\ \ \kappa' \end{bmatrix}$$

are functions of ω^2 and can be written in the polynomial form

$$H_{\alpha\beta}\begin{bmatrix} k_z,\vec{k}_{||} \\ \kappa\ \ \kappa' \end{bmatrix}\equiv\sum_{l_3'=l_3-1}^{l_3+1}\left[\sum_{l_1',l_2'}\Phi_{\alpha\beta}(l,\kappa;l',\kappa')e^{-i\vec{k}_{||}[\vec{x}(l)-\vec{x}(l')]_{||}}-\delta_{l_3 l_3'}M_\kappa\omega^2\right]e^{-ik_z(l_3-l_3')\pi}$$
$$\equiv H_{\alpha\beta}^{(-1)}\begin{bmatrix}\vec{k}_{||}\\ \kappa\ \ \kappa'\end{bmatrix}e^{-ik_z\pi}+H_{\alpha\beta}^{(0)}\begin{bmatrix}\vec{k}_{||}\\ \kappa\ \ \kappa'\end{bmatrix}+H_{\alpha\beta}^{(1)}\begin{bmatrix}\vec{k}_{||}\\ \kappa\ \ \kappa'\end{bmatrix}e^{ik_z\pi}. \tag{15}$$

It can be shown from (15) that $\underline{H}^{(-1)}$ is adjoint to $\underline{H}^{(1)}$ (i.e., $[\underline{H}^{(1)}]^\dagger=\underline{H}^{(-1)}$) and $\underline{H}^{(0)}$ is hermitian. To simplify (14), we break down the 18-dimensional space into two nine-dimensional subspaces, which are associated with $(\kappa=1,4,5)$ and $(\kappa=2,3,6)$, respectively. With this decomposition, we find that the matrices $\underline{H}$ take the form (see Fig. 6)

$$\underline{H}^{(-1)}=\begin{bmatrix}\underline{0}_{9\times9} & \underline{h}^{(-1)}\\ \underline{0}_{9\times9} & \underline{0}_{9\times9}\end{bmatrix},\quad \underline{H}^{(1)}=\begin{bmatrix}\underline{0}_{9\times9} & \underline{0}_{9\times9}\\ \underline{h}^{(1)} & \underline{0}_{9\times9}\end{bmatrix}, \tag{16}$$

and

$$\underline{H}^{(0)}=\begin{bmatrix}\underline{H}_{11} & \underline{H}_{12}\\ \underline{H}_{21} & \underline{H}_{22}\end{bmatrix}, \tag{17}$$

here $\underline{h}^{(-1)}$, $\underline{h}^{(1)}$, and $\underline{H}_{ij}$ are 9×9 matrices. We define the displacement vectors in the two subspaces (labeled 1 and 2) as

$$\underline{\epsilon}_1=(\epsilon_x(1),\epsilon_y(1),\epsilon_z(1),\epsilon_x(4),\epsilon_y(4),\epsilon_z(4),\epsilon_x(5),\epsilon_y(5),\epsilon_z(5))^T ,$$
$$\underline{\epsilon}_2=(\epsilon_x(2),\epsilon_y(2),\epsilon_z(2),\epsilon_x(3),\epsilon_y(3),\epsilon_z(3),\epsilon_x(6),\epsilon_y(6),\epsilon_z(6))^T . \tag{18}$$

Then, (14) becomes two coupled matrix equations,

$$\underline{h}^{(-1)}e^{-i\pi k_z}\underline{\epsilon}_2+\underline{H}_{11}\underline{\epsilon}_1+\underline{H}_{12}\underline{\epsilon}_2=\underline{0}_{9\times1} , \tag{19}$$

$$\underline{H}_{21}\underline{\epsilon}_1+\underline{H}_{22}\underline{\epsilon}_2+\underline{h}^{(1)}e^{i\pi k_z}\underline{\epsilon}_1=\underline{0}_{9\times1} . \tag{20}$$

Solving for $e^{i\pi k_z}\underline{\epsilon}_1$ in (20) and substituting the solution in (19), we obtain

$$e^{i\pi k_z}\underline{\epsilon}_1=-(\underline{h}^{(1)})^{-1}(\underline{H}_{21}\underline{\epsilon}_1+\underline{H}_{22}\underline{\epsilon}_2) \tag{21a}$$

and

$$e^{i\pi k_z}\underline{\epsilon}_2=(\underline{H}_{12})^{-1}\underline{H}_{11}(\underline{h}^{(1)})^{-1}\underline{H}_{21}\underline{\epsilon}_1+(\underline{H}_{12})^{-1}[\underline{H}_{11}(\underline{h}^{(1)})^{-1}\underline{H}_{22}-\underline{h}^{(1)}]\underline{\epsilon}_2 , \tag{21b}$$

which, together, is an eigenvalue equation for $e^{i\pi k_z}$. Thus, for a given $\vec{k}_{||}$ and ω^2, we can solve for the values of $e^{i\pi k_z}$ and, hence, the complex k_z values and also the eigenvectors $\underline{\epsilon}_1,\underline{\epsilon}_2$ by diagonalizing a 18×18 matrix.[21] The 18 solutions will be labeled $j=1,\ldots,18$ (branches corresponding to a given ω^2 not to be confused with modes of a given $\vec{k}$ in Sec. II).

The above calculation applies only when the inverses of $\underline{H}^{(1)}$ and $\underline{H}_{12}$ exist. However, this does not hold for the entire $\vec{k}_{||}$ plane. In particular, for $\vec{k}_{||}=(k_x,k_y)=(0,0)$, we have the point group C_{2v} as the symmetry group of the wave vector, and one can show that both $\underline{H}^{(1)}$ and $\underline{H}_{12}$ are singular. Thus, modification of our method is necessary. The details are given in Appendix D. We find that in this case phonon modes of different symmetries are decoupled; they are labeled A_1, A_2, B_1, and B_2. The six A_1 modes are longitudinal modes. B_1 and B_2, each containing five modes, are two degenerate sets of transverse modes. One B_1 and one B_2 mode correspond to the nonphysical solutions $k_i=\pm\infty$. The remaining two A_2 modes involve BC displacements only and have no physical significance.

B. Results and discussions

Before discussing our results of the complex phonon dispersion relation, we shall first present a general discussion of their symmetry properties. From the definition of the dynamical matrix (5), we can show that

$$D_{\alpha\beta}\begin{bmatrix}-\vec{k}^*\\ \kappa\ \ \kappa'\end{bmatrix}=\left[D_{\alpha\beta}\begin{bmatrix}\vec{k}\\ \kappa\ \ \kappa'\end{bmatrix}\right]^* \tag{22}$$

and

$$\left[D_{\alpha\beta}\begin{bmatrix}\vec{k}\\ \kappa\ \ \kappa'\end{bmatrix}\right]^*=D_{\beta\alpha}\begin{bmatrix}\vec{k}^*\\ \kappa\ \ \kappa'\end{bmatrix} , \tag{23}$$

where we have used the symmetry properties of $\Phi_{\alpha\beta}(l,\kappa;l',\kappa')$. Using (6) and (22), we have

$$M_k\omega^2\epsilon_\alpha^*(\kappa\,|\,\vec{k},j)=\sum_\kappa D_{\alpha\beta}\begin{bmatrix}-\vec{k}^*\\ \kappa\ \ \kappa'\end{bmatrix}\epsilon_\beta^*(\kappa'\,|\,\vec{k},j) .$$

Thus,

$$\omega^2(\vec{k},j)=\omega^2(-\vec{k}^*,j) . \tag{24}$$

Using the reality of ω^2, (8), and (23) for normalized eigenvectors $\epsilon_\alpha(\kappa\,|\,\vec{k},j)$ (note that they are not necessarily orthogonal for complex $\vec{k}$), we obtain

$$\omega^2(\vec{k},j)=\omega^2(\vec{k}^*,j) . \tag{25}$$

Equations (24) and (25) hold for the complex phonon dispersion relations in general.[21,22] For the (001) orientation, the crystal has the reflection symmetry $x,y\rightarrow-x,-y$. Hence, for real $\vec{k}_{||}$, (24) and (25) lead to (writing $k_z=k_r+ik_i$ and dropping index j)

$$\begin{aligned}\omega^2(k_{||},k_r+ik_i)&=\omega^2(\vec{k}_{||},k_r-ik_i)\\ &=\omega^2(-\vec{k}_{||},k_r-ik_i)\\ &=\omega^2(\vec{k}_{||},-k_r+ik_i)\\ &=\omega^2(\vec{k}_{||},-k_r-ik_i) .\end{aligned} \tag{26}$$

Hence, for a given $\vec{k}_{||}$ and ω^2, the complex k_z solutions can be grouped in the form $\pm k_r\pm ik_i$.

We now give the results of our calculations of the complex phonon dispersion relations of some III-V—compound semiconductors for the (001) orientation. We shall refer to the solution $k_z(\omega^2)$, for fixed $\vec{k}_{||}$ and ω^2, as the complex branches, and label them by j. ($j=1,\ldots,18$ for $\vec{k}_{||}\neq\vec{0}$; $j=1,\ldots,6$ for A_1 symmetry and $\vec{k}_{||}=\vec{0}$; $j=1,\ldots,4$ for B_1 or B_2 symmetry and $\vec{k}_{||}=\vec{0}$). We classify these complex branches as follows:[8]

(i) a real branch ($k_i=0$);

(ii) (a) an imaginary branch of the first kind ($k_i\neq0$, $k_r=0$), and (b) an imaginary branch of the second kind ($k_i\neq0$, $k_r=k_{\max}=2\pi/a$) [sometimes we shall not distinguish between (a) and (b), and refer, then, to just imaginary branches]; and

(iii) a complex branch ($k_r\neq0$, $k_i\neq0$).

In Figs. 9—11 we plot some of the complex phonon dispersion relations for GaAs, AlAs, and InP. Imaginary branches of the first kind, real branches, and imaginary branches of the second kind are plotted in the left-hand, middle, and right-hand panels, respectively. The complex

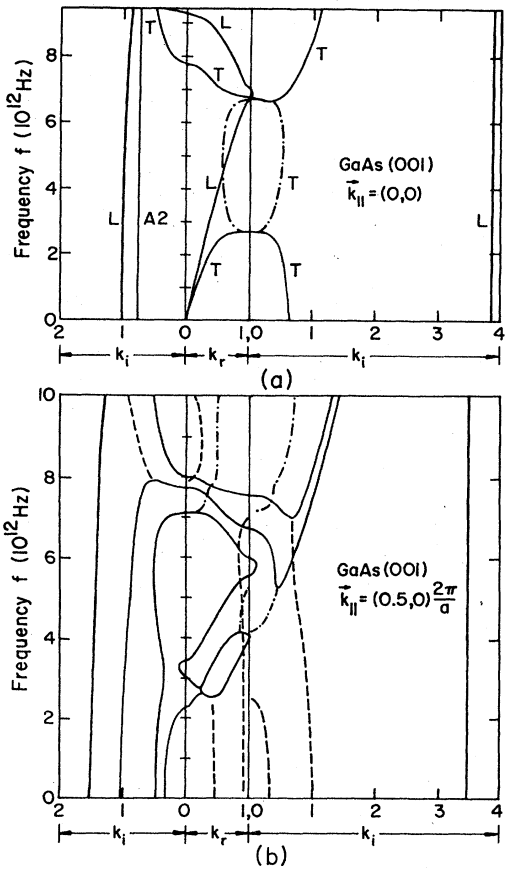

FIG. 9. Complex phonon dispersion relation for GaAs(001). Real and imaginary branches are shown as continuous lines, complex branches are shown as parts of dashed lines. (a) $\vec{k}_{\|}=(0,0)$ and (b) $\vec{k}_{\|}=(2\pi/a)(0.5,0)$.

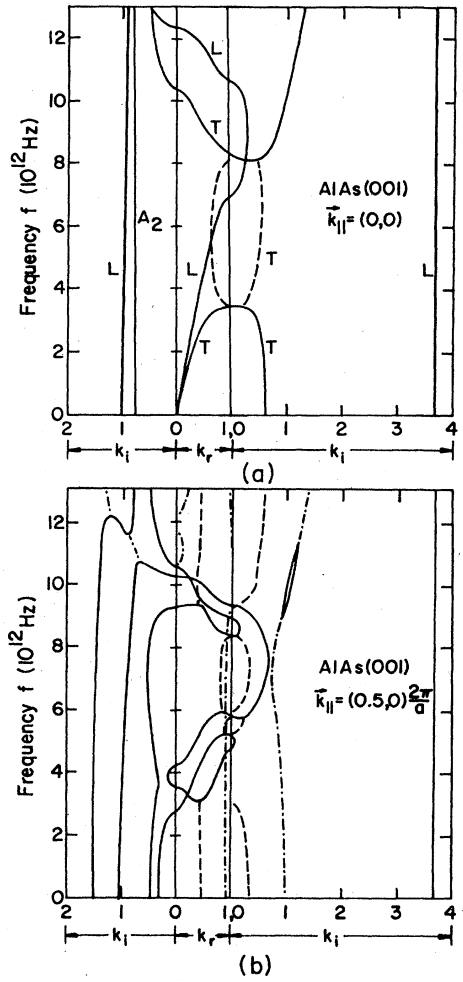

FIG. 10. Complex phonon dispersion relation for AlAs(001). (a) $\vec{k}_{\|}=(0,0)$ and (b) $\vec{k}_{\|}=(2\pi/a)(0.5,0)$.

branches are plotted with their real part in the middle panel, while their imaginary parts are plotted in the left or right panel, according to which of the methods gives clearer topological features. Because of the symmetry relation (26), only the phonon branches with $k_r \geq 0$ or $k_i \geq 0$ are plotted.

We shall follow the terminology of the electronic complex band structure[6] and consider the complex dispersion relation to be sets of (continuous) complex functions $k_z(\omega^2)$; we call these functions real lines. These real lines are observed to obey the same rules as for those in the electronic case.[6,8] These rules are the following:

(i) Real lines cannot terminate nor branch, nor can two or more coalesce into one.

(ii) Real lines cross each other with only vanishing possibility, except when (a) k_z is real or (b) when $k_r=0$ or $k_{\max}$ [possibility (b) was left out in Ref. 6 and was discussed in Ref. 8].

(iii) A real line may loop back to the real k_z axis, and in doing so may enclose a branch point in the complex k_z plane, and join a maximum of $\omega(k_z=k_r)$ of one real branch to the minimum of the next real branch of $\omega(k_z=k_r)$.

(iv) The case corresponding to (iii) for $k_z=ik_i$, $k_r=0$, or $k_{\max}$. For the $\vec{k}_{\|}=\vec{0}$ cases, the branches of different symmetries are independent of one another. Hence they may cross, while those of the same symmetry cannot [see Figs. 9(a), 10(a), and 11(a)]. This independence is destroyed for any arbitrary small value of $\vec{k}_{\|}$ [property (ii)] [see Figs. 9(b), 10(b), and 11(b)].

For the $\vec{k}_{\|}=\vec{0}$ transverse case, all branches are doubly degenerate. Starting at low frequencies we find a real branch and an imaginary branch of the second kind. They connect to each other at the point X and turn into a conjugate pair of complex branches, which, in turn, are connected to each other at the minimum of a real [see Fig. 11(a)] or imaginary branch [see Figs. 9(a) and 10(a)]. Above the optical branches, only imaginary branches are found. For the longitudinal case, we find that the longitudinal-acoustic (LA) and -optical (LO) (real) branches are connected by an imaginary branch of the second kind at point X. The LO branch turns into an imaginary branch of the first kind at point Γ. In addition, we find an imaginary branch of the second kind with large $|k_j|$ which does not connect to any other branch in the frequency range of interest. As mentioned previously,

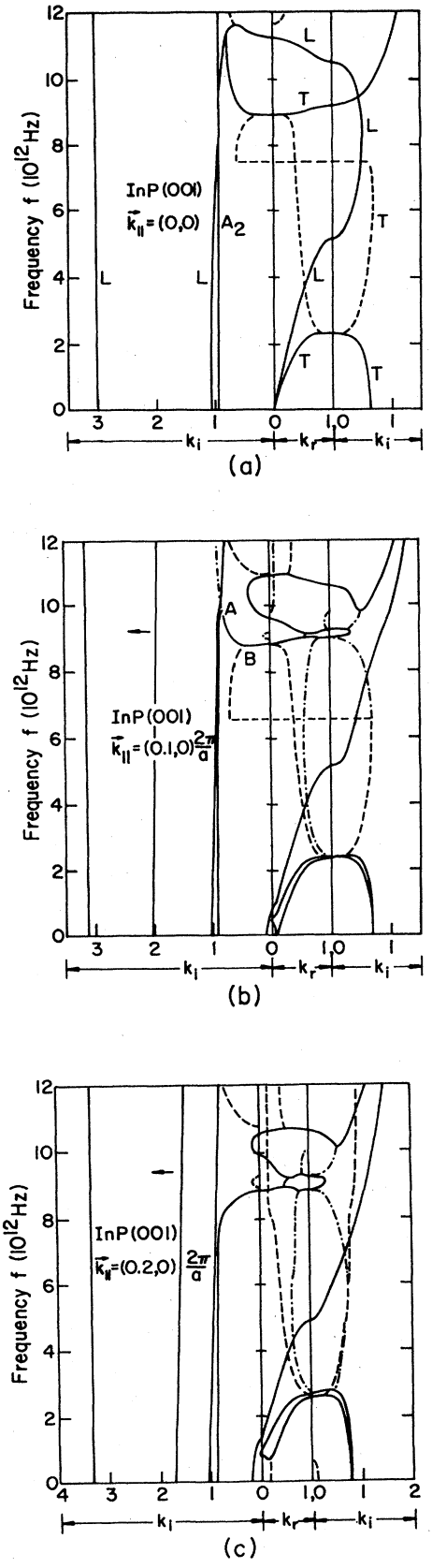

FIG. 11. Complex dispersion relation for InP(001). (a) $\vec{k}_{||}=(0,0)$, (b) $\vec{k}_{||}=(2\pi/a)(0.1,0)$ and (c) $\vec{k}_{||}=(2\pi/a)(0.2,0)$.

the A_2 branch is independent of ω. This branch (marked A_2) is also plotted in Figs. 9(a), 10(a), and 11(a).

The features of the complex phonon dispersion curves for $\vec{k}_{||}\neq\vec{0}$ are much more complicated. Not many features are common to all materials studied. Because the symmetry is reduced, the degenerate transverse branches now split. They may connect to each other, or even to the branches which correspond to longitudinal branches and the nonphysical A_2 branch when $\vec{k}_{||}\to\vec{0}$ [see Figs. 9(b), 10(b), and 11(b)]. We also now have 18 solutions for k_z for fixed $\vec{k}_{||}$ and ω_2. The change in topology of the branches when $\vec{k}_{||}$ deviates slightly from (0,0) is illustrated in Fig. 11, taking InP as an example. A comparison of Fig. 11(a) with Fig. 11(b) shows that most of the main features at low frequencies remain unchanged, except for the aforementioned splitting. At higher frequencies we find crossing of longitudinal branches and transverse branches when $\vec{k}_{||}=\vec{0}$; when $\vec{k}_{||}\neq\vec{0}$, these branches break away from each other to avoid crossing and result in very different topologies. Upon going from $\vec{k}_{||}=(0.1,0)$ to (0.2,0), not much change is observed, except for a maximum (marked A) and a minimum (marked B) of an imaginary branch of the first kind in Fig. 11(b) which coalesces and disappears [near a frequency $(9-10)\times10^{12}$ Hz]. The complex branches that connect to the minimum and the maximum now just connect to each other and form one continuous line, as shown in Fig. 11(c).

Our previous analysis has demonstrated that two complex phonon branches must approach the limit $k_i=\pm\infty$ as $\vec{k}_{||}\to\vec{0}$. Thus only 16 branches are found for $\vec{k}_{||}=\vec{0}$. This interesting feature is also illustrated in Fig. 11. Note that the imaginary branch marked with an arrow moves toward larger values of k_i in Figs. 11(b) and 11(c) as $\vec{k}_{||}$ becomes closer to zero, and eventually disappears in Fig. 11(a).

IV. PHONON DISPERSION RELATIONS FOR AlAs/GaAs(001) SUPERLATTICES

Having obtained the dispersion relations for complex $\vec{k}$ and the associated displacement vectors, we are now ready to calculate the phonon dispersion relations for the superlattice, by "matching" the displacements of the ions and BC's across the interfaces. The same concept should apply for any superlattice, but we shall just perform the calculation for AlAs/GaAs(001) superlattices.

First, we perform the zeroth-order calculation with interaction between ions and BC's of the same range as described in Sec. III. We need to know the force constants among the ions and BC's when the ions are in the superlattice. In principle, this can be obtained by a microscopic theory. However, for our purposes we shall make some assumptions about the force constants. We assume that the charges of all ions and BC's take their values as in their corresponding bulk material, except that of the interfacial As, which is taken to be Z_A+Z_B, where A and B denote AlAs and GaAs, respectively. Recall that our unperturbed calculation involves only short-range forces between neighboring layers of ions, and we assume that all force constants keep their zeroth-order bulk values except

(i) between the interfacial As ion and other ions and BC's, (ii) among the interfacial As ions in the same layer, and (iii) among layers of BC's in the immediate vicinity of the interfacial As ion.

A consideration of the equilibrium condition of the Al and Ga ion nearest the interfacial As ion shows that $\phi_{i\text{-}i}^{(A)'}$ ($\phi_{i\text{-}i}^{(B)'}$) between Al (Ga) ions and these As ions must be the same as in the bulk. We assume that the same holds for $\phi_{i\text{-}i}^{(A)''}$ and $\phi_{i\text{-}i}^{(B)''}$. For the parameters $\phi_{\text{As}}^{(A)''}$, $\phi_{\text{As}}^{(B)''}$, β_{As}, and ψ_{As} involving the interfacial As ions (these parameters play no role in the minimization of energy), we simply take the average between those of the two bulk materials. We assume that the Coulomb interaction between the interfacial As ion and its nearest BC layer in material A, and that between any two BC's in this layer, are associated with an effective dielectric constant ϵ_A'. Similarly, a corresponding quantity is defined for material B. The interaction between the two layers of BC's on opposite sides of the interface is associated with a dielectric constant $\bar{\epsilon}$, which we have taken to satisfy

$$\frac{2}{\bar{\epsilon}}=\frac{1}{\epsilon_A'}+\frac{1}{\epsilon_B'}=\frac{1}{\epsilon_A}+\frac{1}{\epsilon_B}\ , \tag{27}$$

where ϵ_A and ϵ_B are the bulk dielectric constants, $\epsilon_A=10.1$ and $\epsilon_B=13.1$. The dielectric constant for Coulomb interaction between any two As ions in the interface is also taken to be $\bar{\epsilon}$. We choose the remaining force constants $\phi_{\text{As}}^{(A)'}$, $\phi_{\text{As}}^{(B)'}$ involving the interfacial As ion such that the total energy is minimized with the BC's still remaining at the position specified by $p=0.25$. (Note that both GaAs and AlAs gave the same lattice parameter.) Now we consider the minimization of the energy with respect to the displacements of the BC's in material A along the z direction nearest the interfacial As ions. Using the results of Table II (note that it is now necessary to include the "background" terms due to uniformly charged sheets), we found the condition

$$\phi_{\text{As}}^{(A)'}-\phi_1^{(A)'}=\frac{e^1}{t_0^2}\left[2.32\frac{Z_A^2}{\epsilon_A}-4.35\frac{Z_A^2}{\epsilon_A}+Z_AZ_B\left[\frac{2.29}{\epsilon}-\frac{5.79}{\epsilon_A'}\right]+\frac{\sqrt{3}\pi}{4}\left[\frac{2Z_A}{\epsilon}-\frac{Z_A+Z_B}{\epsilon_A'}\right]Z_A\right]\ , \tag{28}$$

where $\phi_1^{(A)'}$ is the unperturbed bulk value of ϕ_1' in A. A similar formula holds for material B. Minimization with respect to the displacements of the As ions along the z direction yields the condition

$$\phi_{\text{As}}^{(A)'}-\phi_{\text{As}}^{(B)'}=\frac{e^2}{t_0^2}\left[5.326\left[\frac{Z_A^2}{\epsilon_A}-\frac{Z_B^2}{\epsilon_B}\right]-7.91\left[\frac{Z_A}{\epsilon_A'}-\frac{Z_B}{\epsilon_B'}\right](Z_A+Z_B)\right]\ . \tag{29}$$

Combining (27)–(29), we find that the energy is minimized when

$$\frac{1}{\epsilon_A'}=0.098 \quad \text{and} \quad \frac{1}{\epsilon_B'}=0.077\ . \tag{30}$$

$\phi_{\text{As}}^{(A)'}$ and $\phi_{\text{As}}^{(B)'}$ are obtained by substituting these values [Eq. (30)] back into (28) and (29).

It should be noted that we did not "derive" the force constants and the dielectric constants at the interface; we simply tried to find the values such that our model would yield physical results ($\omega^2>0$). In principle, we should also consider minimization of energy with respect to displacements in order directions. In view of a similar analysis for the bulk in Sec. III, this consideration will, at most, lead to a small modification in the force constant, and shall be ignored.

With knowledge of the force constants we can now determine the phonon dispersion relations in the superlattice. We still have translational symmetry in the x-y plane, and by considering a fixed $\vec{k}_{||}$, we reduce the problem to that of a one-dimensional chain. The translational period in the z direction is increased. We shall label the superlattice unit cells along the z direction by integers L, and the unit cells of each material by l, with the z component $l_z=1,\ldots,n_\sigma$, where $\sigma=A$ or B denotes the two materials (see Fig. 12).

Consider the displacement eigenvectors for the superlattice for a given $\vec{k}_{||}$ and ω^2. For those ions inside a particular material σ, we can expand the displacement eigenvector in terms of the eigenvectors associated with the complex branches, $f_\alpha^{(\sigma)}(l_3,\kappa\,|\,j)$, of that material σ at the same $\vec{k}_{||}$ and ω^2 as

$$u_\alpha^{(\sigma)}(L,l,\kappa)=e^{i\pi\vec{k}_{||}\cdot\vec{R}_{||}}e^{iqL\pi}\sum_{\sigma,j}C_j^{(\sigma)}f_\alpha^{(\sigma)}(l_3,\kappa\,|\,j)\ , \tag{31}$$

where $C_j^{(b)}$ are the expansion coefficients, and q is the superlattice wave vector in the $\hat{z}$ direction [in units of $2\pi/(n_A+n_B)a$]. We choose j so that we have decreasing $k_i(j)$ with j (recall that k_z appears in groups $\pm k_r\pm ik_i$), and we write

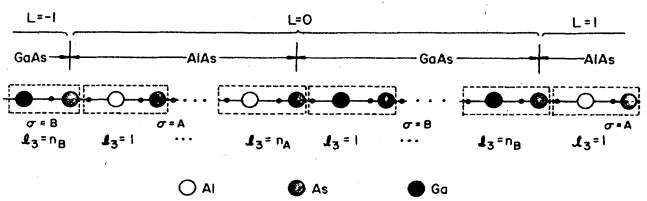

FIG. 12. Schematic diagram for an (n_A/n_B) AlAs/GaAs(001) superlattice. L labels the superlattice unit cell and l_3 labels the principal layer.

$$f_\alpha^{(\sigma)}(l_3,\kappa\,|\,j)=\begin{cases} e^{i[k_z^{(\sigma)}(j)](l_3-1)\pi}\epsilon_\alpha(\kappa\,|\,j) & \text{for } j=1,\ldots,N/2\,, \\ e^{i[k_z^{(\sigma)}(j)](l_3-n_\sigma)\pi}\epsilon_\alpha(\kappa\,|\,j) & \text{for } j=N/2+1,\ldots,N\,, \end{cases} \tag{32}$$

where the $\epsilon_\alpha(\kappa\,|\,j)$ are the solutions obtained as in Sec. III, and N is the number of solutions. In (31) we have chosen the origin of the expansions so that the function $f_\alpha^{(\sigma)}$ always decay away from the origin, and the coefficients $C_j^{(\sigma)}$ will be expected to have the same order of magnitude. The equations of motion for the ions and BC's near the interfaces will allow us to determine the expansion coefficients $C_j^{(\sigma)}$ and q.

We first consider the case where $\underline{h}^{(1)}$ is nonsingular (i.e., $\vec{k}_{||}\neq\vec{0}$ or A_1 modes for $\vec{k}_{||}=\vec{0}$). We shall use the notation established in the preceding section. The equations of motion for the independent displacements $\underline{v}_1^{(\sigma)}(l_3)$ and $\underline{v}_2^{(\sigma)}(l_3)$ in the superlayer layer l_3 of material σ are given in the form of (19) and (20). Those equations for ions and BC's which interact with their neighbors with the same force constants as in the bulk are automatically satisfied when we use the transformation

$$\begin{bmatrix}\underline{v}_1^{(\sigma)}(l_3)\\ \underline{v}_2^{(\sigma)}(l_3)\end{bmatrix}=\begin{bmatrix}\underline{F}_1^{(\sigma)}(l_3)\\ \underline{F}_2^{(\sigma)}(l_3)\end{bmatrix}\underline{C}^{(\sigma)}\,, \tag{33}$$

where $\underline{C}^{(\sigma)}$ is a $(2\nu)\times 1$ column vector with elements $C_j^{(\sigma)}$ defined in (31). ($\nu=9$ for $\vec{k}_{||}\neq\vec{0}$ and $\nu=3$ for the A_1 modes with $\vec{k}_{||}=\vec{0}$.) $\underline{F}_1^{(\sigma)}$ and $\underline{F}_2^{(\sigma)}$ are $\nu\times(2\nu)$ matrices with elements $f_\alpha^{(\sigma)}(l_3,\kappa\,|\,j)$. The expansion (33) is applicable for the displacements of all layers. This can be seen from applying the transfer-matrix method since here we have only modified the interactions between the interface layer and a neighboring principal layer.

The equations of motion corresponding to (19) for $L=0$, $l_3=1$, and $\sigma=A$ and B are given by

$$e^{-iq\pi}\underline{h}_{AB}^{(-1)}\underline{v}_2^{(B)}(n_B)+\underline{\tilde{H}}_{11}^{(A)}\underline{v}_1^{(A)}(1)+\underline{H}_{12}^{(A)}\underline{v}_2^{(A)}(1)=\underline{0}_{\nu\times 1} \tag{34a}$$

and

$$\underline{h}_{BA}^{(-1)}\underline{v}_2^{(A)}(n_A)+\underline{\tilde{H}}_{11}^{(B)}\underline{v}_1^{(B)}(1)+\underline{H}_{12}^{(B)}\underline{v}_2^{(B)}(1)=\underline{0}_{\nu\times 1}\,. \tag{34b}$$

Similarly, the equations of motion corresponding to (20) for $L=0$, $\sigma=A$, and $l_3=n_A$, and $L=-1$, $\sigma=B$, and $l_3=n_B$ are given by

$$\underline{H}_{21}^{(A)}\underline{v}_1^{(A)}(n_A)+\underline{\tilde{H}}_{22}^{(A)}\underline{v}_2^{(A)}(n_A)+\underline{h}_{AB}^{(1)}v_1^{(B)}(1)=\underline{0}_{\nu\times 1} \tag{35a}$$

and

$$\underline{H}_{21}^{(B)}\underline{v}_1^{(B)}(n_B)+\underline{\tilde{H}}_{22}^{(B)}\underline{v}_2^{(B)}(n_B)+e^{iq\pi}\underline{h}_{BA}^{(1)}\underline{v}_1^{(A)}(1)=\underline{0}_{\nu\times 1}\,, \tag{35b}$$

where $\underline{\tilde{H}}_{11}$ and $\underline{\tilde{H}}_{22}$ are modified from their bulk values, $\underline{H}_{11}$ and $\underline{H}_{22}$, due to the presence of interfaces. With the use of (33), the two sets of equations [Eqs. (34) and (35)] can be cast into a (2ν)-dimensional matrix equation,

$$\begin{bmatrix}\underline{Y}_{11} & \underline{Y}_{12}\\ \underline{Y}_{21} & \underline{Y}_{22}\end{bmatrix}\begin{bmatrix}\underline{C}^{(A)}\\ \underline{C}^{(B)}\end{bmatrix}=\underline{0}_{2\nu\times 1}\,, \tag{36}$$

where

$$\underline{Y}_{11}=\begin{bmatrix}\underline{\tilde{H}}_{11}^{(A)}\underline{F}_1^{(A)}(1)+\underline{H}_{12}^{(A)}\underline{F}_2^{(A)}(1)\\ \underline{H}_{21}^{(A)}\underline{F}_1^{(A)}(n_A)+\underline{\tilde{H}}_{22}^{(A)}\underline{F}_2^{(A)}(n_A)\end{bmatrix}\,,$$

$$\underline{Y}_{12}=\begin{bmatrix}\underline{h}_{AB}^{(-1)}\underline{F}_2^{(B)}(n_B)e^{-iq\pi}\\ \underline{h}_{AB}^{(1)}\underline{F}_1^{(B)}(1)\end{bmatrix}\,,$$

$$\underline{Y}_{21}=\begin{bmatrix}\underline{h}_{BA}^{(-1)}\underline{F}_2^{(A)}(n_A)\\ \underline{h}_{BA}^{(1)}\underline{F}_1^{(A)}(1)e^{iq\pi}\end{bmatrix}\,,$$

and $\underline{Y}_{22}$ is in the same form as $\underline{Y}_{11}$ with the index A replaced by B. Equation (36) is a polynomial equation of $e^{-iq\pi}$, which can be solved for each fixed value of ω^2.

We can solve the problem, for a given $\vec{k}_{||}$, by fixing ω^2 and calculating the possible real values of q which satisfy (36). This procedure avoids a self-consistency calculation as used in Ref. 7, and is more efficient in obtaining the phonon dispersion curves. However, it has the disadvantage that, since the phonon branches for the superlattice are quite flat, it is not easy to locate the branches by finding the ω^2 which allow real q's. This problem is particularly serious in the high-frequency region and when the number of layers of the superlattice is large, in which case we expect flat phonon branches.

Note that we have used the information from two interfaces to obtain the matrix equation (36). It is also possible to relate $\underline{C}^{(A)}$ to $\underline{C}^{(B)}$ using only the information from one interface, say, the one between $L=-1$ and $L=0$. However, the matrices involved would contain very large and very small numbers when the superlattice unit cell becomes large. This would cause serious numerical problems in solving q.

For the case where the phonon branches are dispersionless, we will fix q and search for the zeros in the determinant of the matrix $\underline{Y}$ in (36) as a function of ω^2. In principle, this can be done by varying ω^2 until one eigenvalue of the matrix $\underline{Y}$ vanishes. In practice, the solutions are very difficult to find because the eigenvalues of the matrix $\underline{Y}$ are not smooth functions of ω^2. Furthermore, since $\underline{Y}$ is not Hermitian, its eigenvalues are, in general, complex. This makes it difficult to find the zeros by an interpolation method, which usually works for real functions. To circumvent the difficulty, we multiply the matrix $\underline{Y}$ in (36) by a matrix $\underline{G}^\dagger$ to obtain a new matrix $\underline{X}$, where

$$\underline{G}^\dagger=\begin{bmatrix}\underline{G}_A^\dagger & \underline{0}\\ \underline{0} & \underline{G}_B^\dagger\end{bmatrix}\,, \tag{37}$$

where

$$\underline{G}_A = \begin{bmatrix} \underline{F}_1^{(A)}(1) \\ \underline{F}_2^{(A)}(n_A) \end{bmatrix} \text{ and } \underline{G}_B = \begin{bmatrix} \underline{F}_1^{(B)}(1) \\ \underline{F}_2^{(B)}(n_B) \end{bmatrix} .$$

It can be shown that the new matrix $\underline{X}$ is Hermitian. In fact, $\underline{X}$ is simply the dynamical matrix with the mass term subtracted ($\underline{D}-m_\kappa\omega^2\underline{\mathbb{1}}$), transformed in the "new" basis defined by

$$\phi_j^{(\sigma)} = \sum_{\alpha,\kappa,l_3} f_\alpha^{(\sigma)}(l_3,\kappa\,|\,j)\psi_\alpha^{(\sigma)}(\kappa,l_3), \quad \sigma=A,B \tag{38}$$

where the $\psi_\alpha^{(\sigma)}(\kappa,l_3)$ denote the "old" basis vectors. We find that the eigenvalues of $\underline{X}$ are smooth functions of ω^2, and because they are real, it is quite easy to find the zeros by an interpolation method. It should be noted that some "extra" solutions may be found which correspond to the zeros of

$$\det(\underline{G})=\det(\underline{G}_A)\det(\underline{G}_B) .$$

These solutions must be discarded if they do not satisfy (36). In all cases it is vanishingly possible to find $\det(\underline{G})=0$ and $\det(\underline{Y})=0$ simultaneously. Thus it is safe to discard all the roots of $\det(\underline{G})$. The method discussed above is a generalization of the method reported in Ref. 7.

The $\vec{k}_{||}=\vec{0}$ cases again need special attention and are treated in Appendix D.

So far we have only obtained the unperturbed solution. We now proceed to add the correction due to interlayer long-range Coulomb interactions. Because of the complication of the periodicity and dielectric constants, it is tedious to include the correction due to all other layers. Thus, in the perturbation, we shall simply include the Coulomb interaction between all layers of charges with interplanar distance $\leq a/2$. The Coulomb force between ions or BC's is divided by the "dielectric constants" according to the same rule as described in the beginning of this section. We assume that the "correct" first derivatives of the short-range interaction potentials are the same as those of the full BCM. Care is taken to modify the dynamical matrix elements of an ion or BC with itself, due to translational symmetry (see Appendix A). We remark that our ways of including the perturbing Coulomb forces are not unreasonable as the Coulomb matrix elements are extremely tiny for interlayer distances $\geq a/2$; for the short-range interaction potentials we believe that they will be near their bulk values, provided the superlattice layers are not too thin.

The result of the calculation for a (2/2) and a (5/2) AlAs/GaAs(001) superlattice for the $\vec{k}_{||}=\vec{0}$ case is illustrated in Figs. 13 and 14, respectively. Upon comparison with the phonon dispersion curves in Fig. 7, we note that the superlattice branches always appear in frequency regions where at least one of the bulk materials has a real branch.

In the region where the phonon frequencies of the two materials overlap, the qualitative behavior of the superlattice phonon dispersions can be inferred from the "branch folding" of the phonon curves of the bulk materials. In this case, the "mini gaps introduced by the superlattice are negligibly small for reasonably large unit-cell sizes (see Fig. 14). In the frequency region where only the phonon

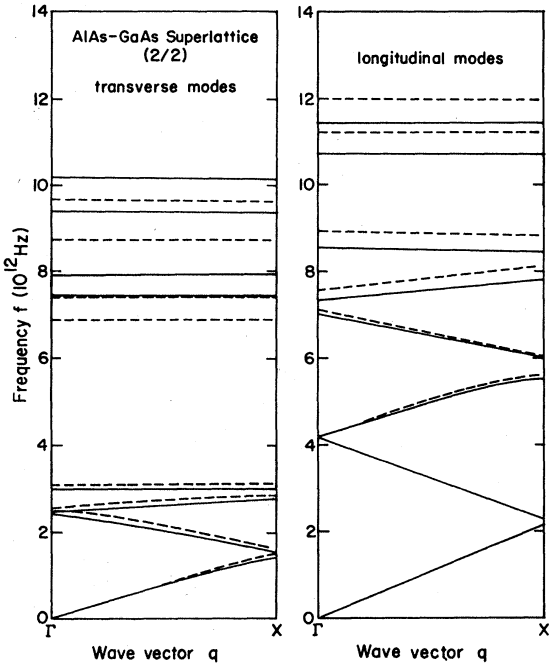

FIG. 13. Phonon dispersion relation of (2/2) AlAs/GaAs(001) superlattice for $\vec{k}_{||}=\vec{0}$. (a) Transverse and (b) longitudinal modes. Dashed curves, unperturbed; solid curves, perturbed.

modes of one material are allowed, the superlattice phonon displacements will be confined in one material, and the dispersion of the phonon frequencies depends on the ratio of the decay length to the width of the barrier ma-

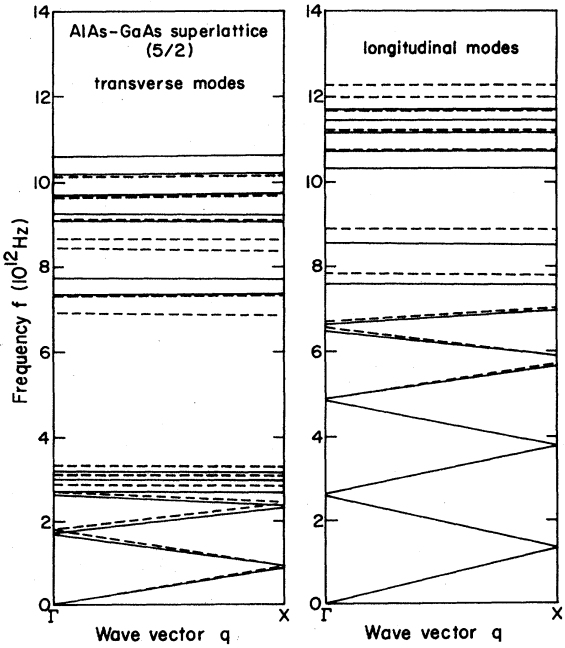

FIG. 14. Phonon dispersion relation of (5/2) AlAs/GaAs(001) superlattice for $\vec{k}_{||}=\vec{0}$. (a) Transverse and (b) longitudinal modes. Dashed curves, unperturbed; solids curves, perturbed.

terial. It is interesting to note that we are in the case where the two materials involved have no overlap in optical frequencies. Thus all the superlattice optical modes are confined in either material. Furthermore, because the decay length ($\lambda \equiv 1/k_i$) of the optical modes is shorter than two layers [the decay length can be inferred from the complex phonon dispersion curves in Figs. 9(a) and 11(a)], these modes are nearly dispersionless [see Figs. 13 and 14]. The transverse-acoustic modes with $f \geq 2.4 \times 10^{12}$ Hz and the longitudinal-acoustic modes with $f \geq 6.3 \times 10^{12}$ Hz are also confined in the AlAs layers. These modes have larger dispersion than the optical modes, because the decay lengths at these frequencies are longer [see Figs. 9(a) and 10(a)].

Recently, Raman measurements on a large number of GaAs/$Al_xGa_{1-x}As$ superlattices have been reported.[3,4,23–25] The measured phonon frequencies for acoustic modes are found to be in good agreement with the model of a layered elastic continuum.[23,24] The optical phonons are less well understood, although a large bulk of experimental data is available. We can compare our theoretical predictions with the existing experimental data for the optical modes. In Fig. 15 we plot the squares of the zero-wave-vector optical-phonon frequencies for AlAs/GaAs superlattices as functions of the inverse square of the GaAs thickness (d_1). The thickness of the AlAs barrier is fixed at four layers (11.3 Å). Because of the short decay lengths of the optical-phonon modes, the increase of the AlAs-barrier thickness has almost no effect on the GaAs-like optical-phonon frequencies. The solid straight lines represent the results predicted by taking the small-q limit of a linear-chain model,[25]

$$\omega^2 = \omega_L^2 - v_s^2 \left[\frac{l\pi}{d_1} \right]^2 ,$$

where l is the folding order, ω_L is the bulk longitudinal-optical- (LO-) phonon frequency, and v_s is the longitudinal sound velocity, which is adjusted to fit our results. We have included in this figure only the four lowest-order frequencies. The experimental data obtained by Colvard *et al.*[25] are superposed. All experimental data are rigidly shifted up by 0.22×10^4 cm^{-2} so that the lowest-order LO-phonon frequency for one sample (with nine GaAs layers) matches our theoretical prediction. This artificial shifting is not unreasonable because both our theoretically predicted and the experimentally measured phonon frequencies have some uncertainties. There is, in general, good agreement between the experimental data and our theoretical predictions. It is interesting to note that all except one experimental datum are associated with odd-order foldings ($l=1$ or 3). The even-order LO-phonon modes may be forbidden in Raman scattering because their displacement eigenvectors have odd parity under the reflection with respect to the x-y plane. The same behavior was also noted for the longitudinal-acoustic- (LA-) phonon modes.[23,24]

In Fig. 16 we plot the squares of the zero-wave-vector optical-phonon frequencies for AlAs/GaAs superlattices as functions of the inverse square of the AlAs thickness

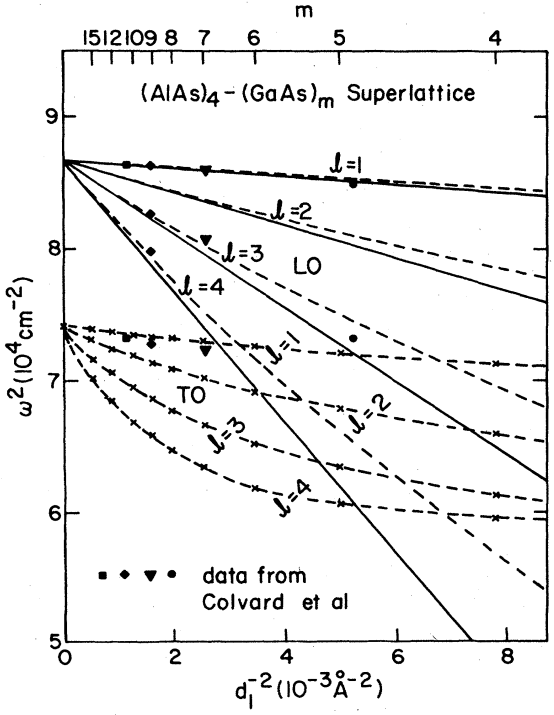

FIG. 15. Squared optical-phonon frequencies of $(AlAs)_4/(GaAs)_m$ ($m=4$–15) superlattices plotted as functions of the inverse square of the GaAs thickness (d_1): longitudinal (—·—·—·—); transverse (-×-×-); linear-chain model (——). The experimental data are taken from Ref. 25.

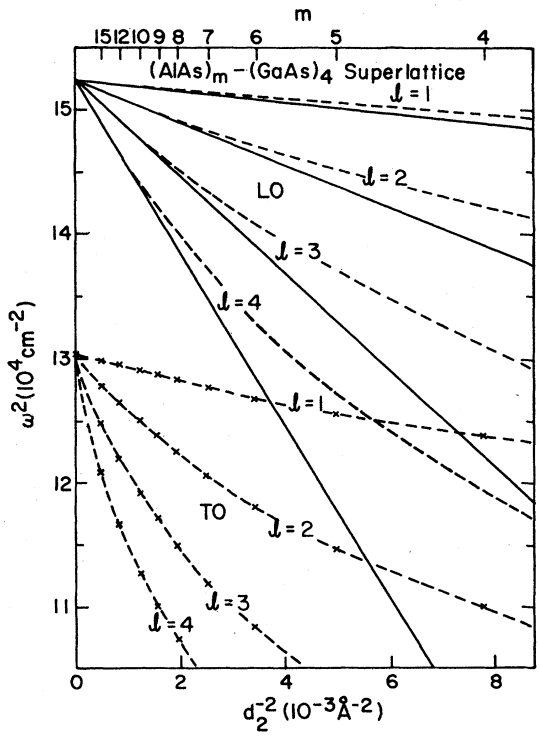

FIG. 16. Squared optical-phonon frequencies of $(AlAs)_m/(GaAs)_4$ ($m=4$–15) superlattice plotted as functions of the inverse square of AlAs thickness (d_2); longitudinal (—·—·—·—); transverse (-×-×-); linear-chain model (——).

(d_2); the GaAs-barrier thickness is fixed at four layers (11.3 Å). Again, the solid straight lines are predictions from a linear-chain model at the small-q limit. Unfortunately, the experimental data of AlAs-like optical-phonon modes are too scarce to allow a meaningful comparison here.

V. SUMMARY

We have used the BCM as an interpolation scheme to obtain the dispersion curves of some heteropolar semiconductors. We have shown that the dispersion curves can be obtained quite accurately, using a perturbation approach, whereas in the zeroth-order approximation only interaction between a finite number of adjacent ions or BC layers exists. Thus, in the zeroth order, we can apply the eigenvalue method to find the complex phonon dispersion relations of the bulk materials, and then, by matching these solutions at the boundaries, we can find the phonon dispersion relations for the AlAs/GaAs superlattices. The correction due to the remaining Coulomb interaction is included in the first-order perturbation theory.

We find that at low frequencies the acoustic-phonon branches are approximately those from a simple "branch folding," but this fails to hold at higher frequencies. In the latter regions phonon modes are found to be very flat.

All optical-phonon branches are found to be dispersionless along the z direction since they are well confined in either material. The theoretical predictions for the optical-phonon frequencies are found to be in good agreement with the existing Raman scattering measurements.

The same method can be extended to superlattices along other directions, and for superlattices made of other semiconductors. The method can also be extended to surface-phonon calculations in materials including long-range Coulomb interactions. We plan to treat these applications in future research work.

ACKNOWLEDGMENTS

We are grateful to M. V. Klein and C. Colvard for many fruitful discussions and for providing us with unpublished experimental data. This work was supported by the University of Illinois Materials Research Laboratory under National Science Foundation Contract No. NSF-DMR-80-20250.

APPENDIX A: DYNAMICAL MATRIX OF THE BCM

We use the notation of Fig. 1. The general form of the short-range (SR) part of the force-constant matrices are

$$\Phi^{\mathrm{SR}}_{\alpha\beta}(l,1;l,3)\equiv\frac{\partial^2\Phi^{\mathrm{SR}}}{\partial X_{l_1,\alpha}\partial X_{l_3,\beta}}=-\begin{bmatrix}\alpha_1 & \beta_1 & \beta_1\\ \beta_1 & \alpha_1 & \beta_1\\ \beta_1 & \beta_1 & \alpha_1\end{bmatrix}, \tag{A1}$$

$$\Phi^{\mathrm{SR}}_{\alpha\beta}(l,3;l,6)=-\begin{bmatrix}\mu_1 & \nu_1 & \delta_1\\ \nu_1 & \mu_1 & \delta_1\\ \bar{\delta}_1 & \bar{\delta}_1 & \lambda_1\end{bmatrix}. \tag{A2}$$

$\Phi^{\mathrm{SR}}_{\alpha\beta}(l2;l,3)$ and $\Phi^{\mathrm{SR}}_{\alpha\beta}(l,1;l,2)$ have the same form as $\Phi^{\mathrm{SR}}_{\alpha\beta}(l,1;l,3)$, with α_1,β_1 in (A1) replaced by α_2,β_2 and α',β', respectively; $\Phi^{\mathrm{SR}}_{\alpha\beta}(l,3;l',6)$ is associated with μ_2, ν_2, δ_2, and λ_2, where l_3 and l'_6 label the BC's surrounding ion 2 (see Fig. 1). The force-constant matrices for the other pairs of ions or BC's follow from symmetry considerations.[5] The self-interaction force-constant matrix is obtained by the requirement of translational invariance,[5]

$$\sum_{l',\kappa'}\epsilon_{l'\kappa'}\Phi^{\mathrm{SR}}_{\alpha\beta}(l,\kappa;l',\kappa')=0\ . \tag{A3}$$

From (A3) we obtain[26] (and analogous formulas for others)

$$\Phi^{\mathrm{SR}}_{\alpha\beta}(l,1;l,1)=4(\alpha'+\alpha_1)\delta_{\alpha\beta}\ ,$$

$$\Phi^{\mathrm{SR}}_{\alpha\beta}(l,3;l,3)=[(\alpha_1+\alpha_2)+2(\mu_1+\mu_2)+(\lambda_1+\lambda_2)]\delta_{\alpha\beta}+[(\beta_1+\beta_2)+(\nu_1+\nu_2)](1-\delta_{\alpha\beta})\ .$$

We adopt the following convention for the dynamical matrix (with distances measured in $a/2$ and wave numbers in $2\pi/a$):

$$D_{\alpha\beta}\begin{bmatrix}\vec{\mathrm{k}} & \\ \kappa & \kappa'\end{bmatrix}\equiv\sum_{l'}\Phi_{\alpha\beta}(l,\kappa;l',\kappa')e^{-i\vec{\mathrm{k}}\cdot[\vec{x}(l)-\vec{x}(l')]\pi}\ .$$

Note that the dynamical matrix is a polynomial in $e^{i\pi k_z}$. The Coulombic part of the dynamical matrix is obtained by Ewald's transformation.[5] The constants introduced in (A1) and (A2) can be expressed in terms of the parameters of the BCM through simple differentiations. We find

$$\alpha'=\tfrac{1}{3}\phi''_{i\text{-}i}+\frac{2}{3}\frac{\phi_{i\text{-}i'}}{t_0},\quad \beta'=\tfrac{1}{3}\phi''_{i\text{-}i}-\frac{1}{3}\frac{\phi'_{i\text{-}i}}{t_0}\ ,$$

$$\alpha_1=\tfrac{1}{3}\phi''_1+\frac{2}{3}\frac{\phi'_1}{r_1}+\frac{B_1}{2},\quad \beta_1=\tfrac{1}{3}\phi''_1-\frac{1}{3}\frac{\phi'_1}{r_1}-\frac{B_1}{2}\ ,$$

$$\mu_1=\nu_1=\frac{B_1}{4}+\frac{\psi''_1}{2},\quad \delta_1=-\lambda_1=\frac{B_1}{4}\ ,$$

and similar equations for parameters associated with ion 2.

APPENDIX B: CALCULATION OF COULOMB ENERGIES BETWEEN LAYERS OF IONS IN THE ZEROTH-ORDER CALCULATION

In this appendix we calculate the Coulomb energy between an ion l,κ and the ion or BC l',κ' of some fixed layer l'. Our method described here is similar to that used by Tong and Maradudin[27] for evaluating the Coulomb part of the dynamical matrix in a surface-phonon calculation. We start with the Poisson sum formulas:

$$\sum_m e^{-(2m+x)^2 t} e^{-i\pi k(2m)} = \sum_m \left[\frac{\pi}{4t}\right]^{1/2} \exp\left[\frac{-\pi^2(k+m)^2}{4t}\right] e^{i\pi(k+m)x}, \tag{B1}$$

$$\sum_m e^{-(2m-1+x)^2 t} e^{-i\pi k(2m-1)} = \sum_m (-1)^m \left[\frac{\pi}{4t}\right]^{1/2} \exp\left[\frac{-\pi^2(k+m)^2}{4t}\right] e^{i\pi(k+m)x}, \tag{B2}$$

which can be obtained by Fourier-transforming either side of the equations. Differentiating (B1) and (B2) with respect to x yields

$$\sum_m (2m+x) e^{-(2m+x)^2} e^{-i\pi k(2m)} = -\frac{i\pi}{2t} \sum_m \left[\frac{\pi}{4t}\right]^{1/2} \exp\left[\frac{-\pi^2(k+m)^2}{4t}\right] (k+m) e^{i\pi(k+m)x}, \tag{B3}$$

$$\sum_m (2m-1+x) e^{-(2m-1+x)^2} e^{-i\pi k(2m-1)} = -\frac{i\pi}{2t} \sum_m (-1)^m \left[\frac{\pi}{4t}\right]^{1/2} \exp\left[\frac{-\pi^2(k+m)^2}{4t}\right] (k+m) e^{i\pi(k+m)x}, \tag{B4}$$

while differentiating with respect to t yields

$$\sum_m (2m+x)^2 e^{-(2m+x)^2 t} e^{-i\pi k(2m)} = \sum_m \frac{2t-\pi^2(k+m)^2}{4t^2} \left[\frac{\pi}{4t}\right]^{1/2} \exp\left[\frac{-\pi^2(k+m)^2}{4t}\right] e^{i\pi(k+m)x}, \tag{B5}$$

$$\sum_m (2m-1+x)^2 e^{-(2m-1+x)^2 t} e^{-i\pi k(2m-1)} = \sum_m (-1)^m \frac{2t-\pi^2(k+m)^2}{2t} \left[\frac{\pi}{4t}\right]^{1/2} \exp\left[\frac{-\pi^2(k+m)^2}{4t}\right]. \tag{B6}$$

We also record some integrals which shall be used below:[28]

$$\int_0^\infty dt\, t^{\nu-1} e^{-\beta/t-\gamma t} = 2\left[\frac{\beta}{\gamma}\right]^{1/2} K_\nu(2\sqrt{\beta\gamma}), \quad \beta,\gamma>0 \tag{B7}$$

$$\int_0^\infty dt \frac{1}{t^{1/2}} e^{-\alpha^2 t} e^{-\beta^2/4t} = \frac{\sqrt{\pi}}{|\alpha|} e^{-|\alpha\beta|}, \quad |\alpha| \neq 0 \tag{B8}$$

$$\int_0^\infty dt \frac{1}{t^{3/2}} e^{-\alpha^2 t} e^{-\beta^2/4t} = \frac{2}{|\beta|} \sqrt{\pi} e^{-|\alpha\beta|}, \quad |\beta| \neq 0 \tag{B9}$$

$$\int_0^\infty dt\, t^{1/2} e^{-\alpha^2 t} e^{-\beta^2/4t} = \frac{\sqrt{\pi}}{2|\alpha|^3}(1+|\alpha\beta|) e^{-|\alpha\beta|}, \quad |\alpha| \neq 0 \tag{B10}$$

$$\frac{1}{\Gamma(\nu)} \int_0^\infty dt\, t^{\nu-1} e^{-xt} = x^{-\nu}, \tag{B11}$$

and the relation

$$K_2(z) = \frac{2}{z} K_1(z) + K_0(z). \tag{B12}$$

We shall choose the basis vectors for the fcc lattice as

$$\vec{a}_1 = (a/2)(1,-1,0), \quad \vec{a}_2 = (a/2)(1,1,0), \quad \vec{a}_3 = (a/2)(1,0,1),$$

and write a lattice vector as

$$\vec{X}(l) = l_1\vec{a}_1 + l_2\vec{a}_2 + l_3\vec{a}_3.$$

The Coulomb energy between a charge l,κ and a layer of charges l',κ' with fixed $l',3$ is

$$S = \sum_{l_1',l_2'} \frac{Z_\kappa Z_{\kappa'} e^2}{\epsilon} \frac{1}{|\vec{X}(l,\kappa) - \vec{X}(l',\kappa')|}. \tag{B13}$$

We note this is a divergent series, and thus calculating it in a direct manner does not work. We need to carry out a transformation analogous to Ewald's transform in three-dimensional space.[5] By translational symmetry, it is sufficient to consider $l=0$, the origin. We then have

$$\vec{x}(0,\kappa) - \vec{x}(l',\kappa') = (a/2)(l_1'+l_2'+l_3',\ l_2'-l_1',\ l_3') + (a/2)(x,y,z),$$

where we have defined

$$\vec{x}(\kappa) - \vec{x}(\kappa') = (a/2)(x,y,z).$$

By a change of variables,

$$\bar{l}_3=-l'_3,\ \bar{l}_2=-l'_2+l'_1,\ \bar{l}_1=-(l'_1+l'_2+l'_3)\ ,$$

one can show that summing over l'_1,l'_2 is equivalent to summing over $\bar{l}_1$ and $\bar{l}_2$ with the restriction that $\bar{l}_1+\bar{l}_2+\bar{l}_3$ be even integers.

Thus (B13) becomes

$$\begin{aligned}S&=\sum_{l_1,l_2}^{(r)}\frac{Z_\kappa Z_{\kappa'}e^2}{\epsilon a/2}\frac{1}{[(\bar{l}_1+x)^2+(\bar{l}_2+y)^2+(\bar{l}_3+z)^2]^{1/2}}\\&=\sum_{\bar{l}_1,\bar{l}_2}^{(r)}\frac{Z_\kappa Z_{\kappa'}e^2}{\epsilon a/2}\frac{1}{\Gamma(\frac{1}{2})}\int_0^\infty dt\exp\{-[(\bar{l}_1+x)^2+(\bar{l}_2+y)^2+(\bar{l}_3+z)^2]^{1/2}\}t^{-1/2}\\&=2\frac{Z_\kappa Z_{k'}e^2}{\epsilon a}\sum_{m,n}f_{mn}e^{-\pi|\bar{l}_3+z|(m^2+n^2)^{1/2}}e^{i\pi(mx+ny)}(m^2+n^2)^{-1/2}\ ,\end{aligned}\tag{B14}$$

where

$$f_{mn}=\begin{cases}[1+(-1)^{m+n}]/2 & \text{for } l_3 \text{ even}\ ,\\ [(-1)^m+(-1)^n]/2 & \text{for } l_3 \text{ odd}\ ,\end{cases}$$

and we have made use of the integrals (B11), (B1), (B2), and (B9). The superscripts (r) in the first two lines remind us of the aforementioned restriction. The sum in (B14), as it stands, is infinite ($m=n=0$ term). This is simply because of the fact that a charge standing in front of a uniformly charged sheet has infinite energy. We shall define these functions $f(d)(2e^2/\epsilon a)$ to be the energy of a unit charge standing a distance d in front of a uniformly charged sheet if unit charge density $f(d)$ is infinite, but which shall cancel out at the end of our calculation. By the physical definition of $f(d)$ (now $d=\frac{1}{2}a/|\bar{l}_3+z|$), we see that it is just the average of S over all x,y, i.e., the $m=n=0$ term in (B14). Thus,

$$S=2\frac{Z_\kappa Z_{\kappa'}e^2}{a\epsilon}\left[f(\tfrac{1}{2}a|\bar{l}_3+z|)+\sum_{m,n}{}'f_{mn}e^{-\pi|\bar{l}_3+z|(m^2+n^2)^{1/2}}e^{i\pi(mx+ny)}\right],\tag{B15}$$

where the prime over the summation sign indicates that the term $m=n=0$ should be omitted.

If $\bar{l}_3+z\neq 0$ (i.e., when the two charges are not on a common sheet), the sum in (B15) is rapidly convergent and can be evaluated numerically.

For the case $\bar{l}_3+z=0$, i.e., $\bar{l}_3=z=0$, we need a further transformation. First note that the factor f_{mn} just restricts our sum to $m+n$ even. Thus,

$$\begin{aligned}S&=\frac{2Z_\kappa Z_{\kappa'}e^2}{a\epsilon}\left[\sum_{m,n}^{(r)}\frac{1}{(m^2+n^2)^{1/2}}e^{i\pi(mx+ny)}+f(0)\right]\\&=\frac{2Z_\kappa Z_{k'}e^2}{\epsilon a}\left[f(0)+\frac{1}{\Gamma(\frac{1}{2})}\int_0^\infty dt\,t^{-1/2}\sum_{m\,(\neq 0)}\sum_n e^{-(4m^2+4n^2)t}e^{i\pi(2nx+2ny)}+\sum_{n\,(\neq 0)}\frac{1}{2|n|}e^{2i\pi ny}\right.\\&\qquad\left.+\frac{1}{\Gamma(\frac{1}{2})}\int dt\,t^{-1/2}\sum_{m,n}\exp\{-4[(m-1/2)^2+(n-1/2)^2]t\}\exp[i\pi(2m-1)x+(2n-1)y]\right]\\&=\frac{2Z_\kappa Z_{k'}e^2}{\epsilon a}\left\{f(0)+\sum_{n=1}^\infty\frac{1}{n}\cos(2\pi ny)+\frac{2}{\sqrt{\pi}}\int_0^\infty dt\,\frac{1}{t^{1/2}}\left[\sum_{m=1}^\infty\sum_n\cos(2m\pi x)e^{-4m^2t}\left[\frac{\pi}{4t}\right]^{1/2}\exp\left[\frac{-\pi^2(y+n)^2}{4t}\right]\right.\right.\\&\qquad+(-1)^n\cos[(2m-1)\pi x]e^{-4(m-1/2)^2t}\left[\frac{\pi}{4t}\right]^{1/2}\\&\qquad\left.\left.\times\exp\left[\frac{-\pi^2(y+m)^2}{4t}\right]\right]\right\}\\&=\frac{2Z_\kappa Z_{\kappa'}e^2}{\epsilon a}\left[f(0)+\sum_{n=1}^\infty n^{-1}\cos 2\pi ny+2\sum_{m=1}^\infty\sum_n\{K_0(2m\pi|y+n|)\cos(2m\pi x)\right.\\&\qquad\left.+(-1)^nK_0((2m-1)\pi|y+n|)\cos[(2m-1)\pi x]\}\right],\end{aligned}\tag{B16}$$

where we have used (B11), (B1), (B2), and (B7). The series in (B16) is rapidly convergent if $y \neq 0$. Thus we can use (B16) for $\bar{l}_3 = z = 0$, as long as $\kappa \neq \kappa'$.

For the case $\bar{l}_3 = 0$ and $\kappa = \kappa'$, we are unable to transform the sum S into a rapidly convergent series. We evaluate it in a straightforward manner by summing over concentric circles of more and more distant neighbors, while subtracting a uniformly charged neutralizing disk with a radius equal to the furthest neighbor included and with a charge equal and opposite to the ions included in the sum. The sum still shows substantial oscillation even when we sum up to radius $\sim 400a/2$. Fortunately, this uncertainty only affects our α_M slightly (about 1%) and does not affect $d\alpha_M/dp$ at all (see below), and thus is sufficiently accurate for our purposes.

The column headed E_C in Table II gives the Coulomb energy (in units of $4Z^2e^2/a$) after subtracting the uniform background terms $f(d)$. The error for $(\bar{l}_3, \kappa, \kappa') = (0,1,1)$ indicates the mentioned uncertainty (roughly). Those terms not recorded can be obtained by symmetry arguments.

One can verify that the uniform background terms $f(d)$ exactly cancel out in our zeroth-order calculation, by using the fact that $f(d) - f(0)$ is linear in d. This is partly the reason for including the Coulomb interaction between layers of ions in the particular way described in Sec. III. Had we included the interactions in a different way, such that some uncanceled $f(d)$ terms are left over, we would obtain infinites for our zeroth-order calculation and an infinite perturbation term for ϕ'_{i-i}, ϕ'_1, and ϕ'_2.

As we see in Eqs. (3) and (4) of Sec. II, we also need the rate of charge of the Coulomb energies with respect to the change in p ($p = 0.25$ for equilibrium positions). We evaluate (B15) and (B16) for two nearby p values; the derivatives are evaluated numerically. We note that the $\bar{l}_3 = 0$, $\kappa = \kappa'$ term does not contribute to the derivative, as noted earlier. The results are presented in the column headed dE_C/dp in Table II.

In principle, we should also need a minimum of energy with respect to displacement of the BC perpendicular to the bonds ($s_\perp a/2$). Thus we also investigate the change in energies when a single charge at $l_3, \kappa = 0,3$, is displaced perpendicular to the bonds. Note that the crystal in equilibrium is invariant under the reflection σ_{da} with respect to the plane containing ion 1 and BC's 3 and 6 (see Fig. 1). Thus the total Coulomb energy is an extremum for displacements normal to the σ_{da} plane. Therefore, we need only consider the change due to the displacement ($s_\perp a/2$) in the σ_{da} plane and perpendicular to the bond. This can be done by slightly modifying the previous machine program, except when $l'_3 = 0$ and $\kappa' = 3$ or 6. For these cases the component of displacement along the z direction produces an extremum by symmetry, since it is originally lying in the plane of the charges (3 and 6 in Fig. 1) with which it is interacting (ignore the term due to the fact that it is an unstable equilibrium). The remaining displacement in the plane can be evaluated again by a slight modification of the previous machine program. (In fact, by symmetry, the term with $\kappa' = 3$ is identically zero.) The result with background terms excluded is included in Table III.

We note also that the total of the uniform background terms under the change of positions of the BC is an (unstable) extremum, and thus we omit it entirely in the present problem. Summing up the terms of Coulomb energies with the results in Tables II and III, we find $\alpha_M = 5.326$ and $d\sigma_M/dp = 2.764$. $\partial E/\partial s_\perp = 0.07(Ze^2/\epsilon a)$, which is much smaller than the other terms entering into our calculations, and can be ignored. Thus, in the zero-order approximation, we need only the new values of α_M and $d\alpha_M/dp$ in (2)–(4), and no further short-range forces need to be introduced.

For reference, we record the corresponding results for group-IV semiconductors in the BCM ($p = 0.0$) in Table IV, which would be useful for covalent semiconductor surface-phonon calculations. We find $\alpha_M = 5.006$, $d\alpha_M/dp = 0.0$, and $\partial E/\partial s_\perp = 0$. The latter two follow from symmetry.

TABLE II. Coulomb energy E_c with the uniform background excluded between a charge $0,\kappa$ and a layer of charges l',κ' with fixed l'_3 and its derivative with respect to p, dE_c/dp for III-V zinc-blende compounds ($p = 0.25$). The energies are measured in $4Z^2e^2/\epsilon a$.

l'_3	κ	κ'	E_C	dE_C/dp
0	1	1	−5.34±0.2	0
0	1	3	−0.069	0.7
0	2	6	−0.91	−3.34
0	3	4	−0.03	−0.03
1	3	4	+0.09	0.66
0	3	6	−0.30	0.83

TABLE III. Change of Coulomb energy between a charge $(l,\kappa) = (0,3)$ and a layer of charges l',κ' with fixed l'_3 (excluding the background terms) with respect to the displacement ($s_\perp$) perpendicular to the bond, $dE_c/ds_\perp$. The energies are measured in $4Z^2e^2/\epsilon a$.

l',κ'	$dE_C/ds_\perp$
0,1	−1.24
0,2	1.84
0,3	0.0
0,4	0.2
0,6	−0.65
1,4	−0.18

TABLE IV. Coulomb energy between a charge $(0,\kappa)$ and a layer of charges (l',κ') with fixed l'_3 for group-IV semiconductors in the BCM ($p = 0.0$). The background terms are excluded. The energies are measured in $4Z^2e/\epsilon a$.

l'_3	κ	κ'	E_c
0	1	1	−5.34±0.02
0	1	3	−0.336
0	3	4	−0.007
0	3	6	−0.403

APPENDIX C: COULOMB MATRIX ELEMENTS

Below we shall show the Coulomb matrix elements between layers of ions considered in Sec. III. In this case the Ewald transformation[5] is not applicable. The method we shall use is similar to that in Ref. 27. Thus in most cases we simply record the results, and only for cases where the method is different shall we elaborate on our procedure. The notation is as in Appendix B.

The Coulomb matrix elements (in units of e^2/v_a, where v_a is the unit-cell volume) are, for $l_3\kappa \neq l_3',\kappa'$,

$$C_{\alpha\beta}\begin{pmatrix} \vec{k}_{\parallel} \\ l_3,\kappa,\ l_3',\kappa' \end{pmatrix} = -2\sum_{\bar{l}_1,\bar{l}_2}^{(r)} \frac{3(\bar{l}+r)_\alpha(\bar{l}+r)_\beta - \delta_{\alpha\beta}r^2}{[(\bar{l}_1+x)^2+(\bar{l}_2+y)^2+(\bar{l}_3+z)^2]^{1/2}} e^{-i\vec{k}_{\parallel}\cdot\vec{x}(\bar{l})}, \tag{C1}$$

where $r_1=x$, $r_2=y$, $r_3=z$, and the suffix (r) represents a restriction that $\bar{l}_1+\bar{l}_2+\bar{l}_3$ be even. In what follows we shall drop the labels $\vec{k}_{\parallel}$, $l3,\kappa$, $l3',\kappa'$. We shall consider three different cases:

Case I: $\bar{l}_3+z\neq 0$. We define

$$g(m,n)\equiv \exp\{-\pi\,|\,\bar{l}_3+z\,|\,[(k_1+m)^2+(k_2+n)^2]^{1/2}\}\exp\{i\pi[(k_1+m)x+(k_2+n)y]\},$$

where k_1 and k_2 are the x and y components of $\vec{k}_{\parallel}$. Then, we have

$$C_{xx}=2\pi^2\sum_{m,n} f_{mm}(k_1+m)^2[(k_1+m)^2+(k_2+n)^2]^{-1/2}g(m,n), \tag{C2}$$

$$C_{xy}=2\pi^2\sum_{m,n} f_{mm}(k_1+m)(k_2+n)[(k_1+m)^2+(k_2+n)^2]^{-1/2}g(m,n), \tag{C3}$$

$$C_{xz}=i2\pi^2\sum_{m,n} f_{mn}(k_1+m)\frac{\bar{l}_3+z}{|\,\bar{l}_3+z\,|}g(m,n). \tag{C4}$$

C_{yy} and C_{yz} are identical in form to C_{xx} and C_{xz} with the interchange of x and y, and the interchange of k_1 and k_2,

$$C_{zz}=-(C_{xx}+C_{yy}). \tag{C5}$$

Case II: $l_3=l_3'$, $z=0$, *but* $\kappa\neq\kappa'$. In this case, $\bar{l}_1+x,\bar{l}_2+y$ never vanishes. Thus we can use (C1) and (B12) to obtain

$$C_{xx}=-\frac{2}{\Gamma(\frac{5}{2})}\sum_{\bar{l}_1,\bar{l}_2}^{(r)}\int_0^\infty dt\,t^{3/2}[2(\bar{l}_1+x)^2-(\bar{l}_2+y)^2]e^{[(\bar{l}_1+x)^2+(\bar{l}_2+y)^2]t}e^{i\pi(k_1\bar{l}+k_2\bar{l}_2)}.$$

Adopting (B1), (B2), (B5), and (B6) for the sum over $\bar{l}_1$ gives

$$C_{xx}=-\frac{2}{\Gamma(\frac{5}{2})}\sum_{m,\bar{l}_2}(-1)^{m\bar{l}_2}\int_0^\infty dt\,t^{3/2}\left[\frac{2t-\pi^2(k_1+m)^2}{2t^2}-(\bar{l}_2+y)^2\right]\left[\frac{\pi}{4t}\right]^{1/2}e^{-\pi^2(k_1+m)^2/4t}e^{-(\bar{l}_2+y)^2t}e^{i\pi[(k_1+m)x-k_2\bar{l}_2]}.$$

With use of (B7) and (B11), we obtain

$$C_{xx}=2\pi^2\sum_{m,\bar{l}_2}(-1)^{m\bar{l}_2}(k_1+m)^2K_0(\pi\,|\,\bar{l}_2+y\,|\;|\,k_1+m\,|)e^{i\pi[(k_1+m)x-k_2\bar{l}_2]}. \tag{C6}$$

Similarly, for C_{xy} we obtain

$$C_{xy}=-\frac{2}{\Gamma(\frac{5}{2})}\sum_{\bar{l}_1,\bar{l}_2}^{(r)}\int_0^\infty dt\,t^{3/2}[3(\bar{l}_1+x)(\bar{l}_2+y)]e^{-[(\bar{l}_1+x)^2+(\bar{l}_2+y)^2]t}e^{i\pi(k_1\bar{l}_1+k_2\bar{l}_2)}.$$

Adopting (B5) and (B6) for the sum over $\bar{l}_1$, and using (B7), we obtain

$$C_{xy}=i2\pi^2\sum_{m,\bar{l}_2}(-1)^{m\bar{l}_2}(k_1+m)\,|\,k_1+m\,|\,\frac{\bar{l}_2+y}{|\,\bar{l}_2+y\,|}K_1(\pi\,|\,k_1+m\,|\;|\,\bar{l}_2+y\,|)e^{i\pi[(k_1+m)x-k_2\bar{l}_2]}. \tag{C7}$$

From (C1), we have

$$C_{xz}=C_{yz}=0.$$

C_{yy} is identical in form to C_{xx} in (C8) with x,y interchanged and k_1,k_2 interchanged,

$$C_{zz}=-(C_{zz}+C_{yy}). \tag{C8}$$

Case III: $l_3=l_3'$ *and* $\kappa=\kappa'$. In this case we have $x=y=z=0$. This is the same situation as in Ref. 27. Thus we have, by translational invariance,

$$C_{\alpha\beta}\begin{bmatrix}\vec{k}_{||}\\ l_3,\kappa,\ l_3,\kappa\end{bmatrix}=C^{(1)}_{\alpha\beta}\begin{bmatrix}\vec{k}_{||}\\ l_3,\kappa,\ l_3,\kappa\end{bmatrix}-\sum_{l_3'',\kappa''\neq l_3,\kappa}C_{\alpha\beta}\begin{bmatrix}0\\ l_3,\kappa,\ l_3'',\kappa''\end{bmatrix}, \tag{C9}$$

where $C^{(1)}_{\alpha\beta}$ is given by (C1) with the omission of the $\bar{l}_1=\bar{l}_2=0$ term. We have

$$C^{(1)}_{xx}=-\tfrac{8}{3}[g_1(k_1,k_2)-\tfrac{1}{2}g_1(k_2,k_1)+g_2(k_1,k_2)-\tfrac{1}{2}g_2(k_2,k_1)], \tag{C10}$$

where

$$g_1(k_1,k_2)\equiv\sum_{m=1}^{\infty}\sum_{n=-\infty}^{\infty}\cos(2\pi mk_1)\left[\pi^2(k_2+n)^2K_0(2m\pi\,|\,k_2+n\,|\,)+\frac{\pi\,|\,k_2+n\,|}{m}K_1(2m\pi\,|\,k_2+n\,|\,)\right]$$

and

$$g_2(k_1,k_2)\equiv\sum_{m=1}^{\infty}\sum_{n=-\infty}^{\infty}(-1)^n\cos[(2m-1)\pi k_1]\left[\pi^2(k_2+n)^2K_0((2m-1)\pi\,|\,k_2+n\,|\,)+\frac{2\pi\,|\,k_2+n\,|}{2m-1}K_1((2m-1)\pi\,|\,k_2+n\,|\,)\right],$$

$$C^{(1)}_{xy}=4\pi^2\left[\sum_{n=1}^{\infty}\sum_{m=-\infty}^{\infty}(k_1+m)\,|\,k_1+m\,|\,\{\sin(2n\pi k_2)K_1(2n\pi\,|\,k_1+m\,|\,)+(-1)^m\sin[(2n-1)\pi k_2]K_1((2n-1)\pi\,|\,k_1+m\,|\,)\}\right], \tag{C11}$$

$$C^{(1)}_{xy}=C^{(1)}_{yz}=0\,.$$

$C^{(1)}_{yy}$ is given by (C10) with k_1 and k_2 interchanged, and

$$C^{(1)}_{zz}=-(C^{(1)}_{xx}+C^{(1)}_{yy})\,. \tag{C12}$$

APPENDIX D: THE SPECIAL CASE OF $\vec{k}_{||}=\vec{0}$

In this appendix we shall show in some detail the modifications necessary for the calculation of the bulk complex phonon relations and superlattice dispersion curves when $\vec{k}_{||}=\vec{0}$.

First, we show, due to symmetry, that $\underline{H}^{(1)}$ and $\underline{H}_{12}$ are singular. We then make use of the very same symmetry to provide the modification necessary to our method of calculation. The general form of $H^{(1)}_{\alpha\beta}$ is

$$H^{(1)}_{\alpha\beta}\begin{bmatrix}0\\3\ \ 4\end{bmatrix}=\begin{bmatrix}a & b_1 & b_2\\ b_3 & c & d\\ b_4 & d & e\end{bmatrix},$$

and

$$H^{(1)}_{\alpha\beta}\begin{bmatrix}0\\3\ \ 5\end{bmatrix},\ H^{(1)}_{\alpha\beta}\begin{bmatrix}0\\6\ \ 4\end{bmatrix},\ H^{(1)}_{\alpha\beta}\begin{bmatrix}0\\6\ \ 5\end{bmatrix}$$

can be obtained by the following symmetry argument: If $\underline{R}$ is a symmetry operator which transforms κ_1,α, κ_2,β and $\vec{k}$ into $\kappa_1'\alpha'$, κ_2',β' and $\underline{R}\vec{k}$, respectively, then

$$D_{\alpha'\beta'}\begin{bmatrix}\underline{R}\vec{k}\\ \kappa_1'\ \ \kappa_2'\end{bmatrix}=D_{\alpha\beta}\begin{bmatrix}\vec{k}\\ \kappa_1\ \ \kappa_2\end{bmatrix}.$$

Thus,

$$H^{(1)}_{\alpha\beta}\begin{bmatrix}0\\3\ \ 5\end{bmatrix}=\begin{bmatrix}c & b_3 & d\\ b_1 & a & b_2\\ d & b_4 & e\end{bmatrix},$$

and

$$H^{(1)}_{\alpha\beta}\begin{bmatrix}0\\6\ \ 5\end{bmatrix},\ H^{(1)}_{\alpha\beta}\begin{bmatrix}0\\6\ \ 4\end{bmatrix}$$

follows from

$$H^{(1)}_{\alpha\beta}\begin{bmatrix}0\\3\ \ 4\end{bmatrix},\ H^{(1)}_{\alpha\beta}\begin{bmatrix}0\\3\ \ 5\end{bmatrix},$$

respectively, by changing the signs of the xz, yz, zx, and zy components. In our model, we also have

$$H^{(1)}_{\alpha\beta}\begin{bmatrix}\vec{k}_{||}\\1\ \ 4\end{bmatrix}=H^{(1)}_{\alpha\beta}\begin{bmatrix}\vec{k}_{||}\\1\ \ 5\end{bmatrix}=0\,.$$

With these observations and some algebra, we can show that $\det\underline{h}^{(1)}=\det\underline{h}^{(-1)}=0$. Thus our previous method does not apply. A similar argument shows that $\det\underline{H}_{12}=0$. In fact, if we have a strictly short-range interaction model (such as that in Sec. II), $\underline{h}^{(1)}$ is singular for the entire $k_x=k_y$ line in the $\vec{k}_{||}$ plane.

Thus for the $\vec{k}_{||}=\vec{0}$ case, the modification of our method is necessary. We observe that the source of the trouble is symmetry: for $\vec{k}_{||}=\vec{0}$, the BC's $\kappa=3,6,\kappa=4,5$

are, in a sense, "equivalent" to each other, and thus lead to linear dependent rows and columns in the matrix $\underline{h}^{(1)}$. Thus we proceed by applying group theory to eliminate the "redundant" degrees of freedom. Consider the 18 displacements $\epsilon_x(\kappa)$. They form a basis for a 18×18 representation of the group of the wave vector $\vec{k}=k_z\hat{z}$, C_{2v}. The character table is presented as Table V. From that, we can decompose the 18×18 representation into

$$6A_1+2A_2+5B_1+5B_2 .$$

The displacements associated with these irreducible representations are [in the form $(\epsilon_x(1), \epsilon_y(1), \epsilon_z(1), \epsilon_x(2), \ldots, \epsilon_z(6))$], for A_1,

TABLE V. Character table of the group of the wave vector $\vec{k}=k_z\hat{z}$, C_{2v}. The notation is that of Ref. 29.

	E	C_{2z}	σ_{da}	σ_{db}
A_1	1	1	1	1
A_2	1	1	−1	−1
B_1	1	−1	1	−1
B_2	1	−1	−1	1
$\epsilon_\alpha(\kappa)$	18	−2	4	4

$$(0, 0, \epsilon_z(1), 0, 0, \epsilon_z(2), \epsilon_x(3), \epsilon_x(3), \epsilon_z(3), \epsilon_x(4), -\epsilon_x(4), \epsilon_z(4), -\epsilon_x(4), \epsilon_x(4), \epsilon_z(4), -\epsilon_x(3), -\epsilon_x(3), \epsilon z(3)) , \tag{D1}$$

for A_2,

$$(0, 0, 0, 0, 0, 0, \epsilon_x(3), -\epsilon_x(3), 0, \epsilon_x(4), \epsilon_x(4), 0, -\epsilon_x(4), -\epsilon_x(4), 0, -\epsilon_x(3), +\epsilon_x(3), 0) , \tag{D2}$$

for B_1,

$$(\epsilon_x(1), \epsilon_x(1), 0, \epsilon_x(2), \epsilon_x(2), 0, \epsilon_x(3), \epsilon_x(3), \epsilon_z(3), \epsilon_x(4), \epsilon_x(4), 0, \epsilon_x(4), \epsilon_x(4), 0, \epsilon_x(3), \epsilon_x(3), -\epsilon_z(3)) , \tag{D3}$$

and for B_2,

$$(\epsilon_x(1), -\epsilon_x(1), 0, \epsilon_x(2), -\epsilon_x(2), 0, \epsilon_x(3), -\epsilon_x(3), 0, \epsilon_x(4), -\epsilon_x(4), \epsilon_z(4), \epsilon_x(4), -\epsilon_x(4), -\epsilon_z(4), \epsilon_x(3), -\epsilon_x(3), 0) . \tag{D4}$$

A_1 corresponds to longitudinal modes. B_1 and B_2 correspond to (degenerate) transverse modes. The "longitudinal" and "transverse" modes are defined according to the directions of the ionic displacements. Numerical solutions show that the displacements of the BC's are not "pure" in these modes. For A_2 symmetry, we find that the adiabatic condition leads to two purely imaginary branches which are independent of ω^2. Furthermore, because these modes have symmetries different from the others, they play no role in the superlattice dispersion-relation calculations and are physically irrevelant.

We are now ready for the complex phonon-dispersion-relation calculation for $\vec{k}_{||}=\vec{0}$. First, consider the A_1 case. The displacement vectors of the A_1 mode are determined by six independent components which we denote by the set

$$S_A=\{\epsilon_z(1), \epsilon_x(4), \epsilon_z(4), \epsilon_z(2), \epsilon_x(3), \epsilon_z(3)\}$$

[see (D1)]. The equation of motion for the A_1 mode is given by

$$0=\sum_{\sigma=-1}^{+1}\sum_{\kappa',\beta}(H_{\alpha\beta}^{(\sigma)})^{\text{eff}}\begin{bmatrix}0\\ \kappa & \kappa'\end{bmatrix}e^{i\pi k_z\sigma}\epsilon_\beta(\kappa') , \tag{D5}$$

where $\epsilon_\alpha(\kappa)$ and $\epsilon_\beta(\kappa')$ belong to the set S_A. We have

$$(H_{\alpha\beta}^{(\sigma)})^{\text{eff}}\begin{bmatrix}0\\ \kappa & \kappa'\end{bmatrix} ,$$

the "effective" dynamical matrix defined by

$$(H_{\alpha\beta}^{(\sigma)})^{\text{eff}}\begin{bmatrix}0\\ \kappa & \kappa'\end{bmatrix}=\sum_{\kappa'',\beta''}^{(e)}H_{\alpha\beta'}^{(\sigma)}\begin{bmatrix}0\\ \kappa & \kappa''\end{bmatrix}\text{sgn}(\kappa',\beta;\kappa'',\beta'') , \tag{D6}$$

where the κ'',β'' label the components $\epsilon_{\beta''}(\kappa'')$ which are related to $\epsilon_\beta(\kappa')$ by the symmetry operations of C_{2v}, and $\text{sgn}(\kappa',\beta;\kappa'',\beta'')=\pm 1$ according to $\epsilon_\beta(\kappa')=\pm\epsilon_{\beta''}(\kappa'')$, as required by symmetry [see (D1)]. Equation (D5) contains all independent equations in (14), as one can convince himself that (i) if $\tilde{\kappa},\tilde{\alpha}$ is related to κ,α by a symmetry operation, then the equation of motion of $\tilde{\kappa},\tilde{\alpha}$ in (20) is the same as that of κ,α, and (ii) if $\epsilon_\alpha(\kappa)=0$, then (D5) is automatically satisfied as

$$(H_{\alpha\beta}^{(\sigma)})^{\text{eff}}\begin{bmatrix}0\\ \kappa & \kappa'\end{bmatrix}=0$$

for each $\epsilon_\beta(\kappa')$ belonging to S_A, and thus no further restriction of $\epsilon_\beta(\kappa')$ is needed. With the decomposition

$$\underline{\epsilon}_1=\begin{bmatrix}\epsilon_z(1)\\ \epsilon_x(4)\\ \epsilon_z(4)\end{bmatrix}, \quad \underline{\epsilon}_2=\begin{bmatrix}\epsilon_z(2)\\ \epsilon_z(3)\\ \epsilon_z(3)\end{bmatrix} ,$$

and following the same argument in deriving (21), we obtain a 6×6 eigenvalue equation [in place of (21)]. For each ω^2, we obtain six eigenvalues for $e^{ik_z\pi}$ and six eigenvectors.

For B_1 (or B_2) symmetry, we have, according to (D3) [or (D4)], five independent displacements,

$$S_B=\{\epsilon_x(1),\epsilon_x(4),\epsilon_z(4),\epsilon_x(2),\epsilon_x(3)\}\ .$$

Equations corresponding to (D6), (15)–(17), (19), and (20) can be written, with the decomposition [in place of (18)]

$$\underline{\epsilon}_1=\begin{bmatrix}\epsilon_x(1)\\ \epsilon_x(4)\\ \epsilon_z(4)\end{bmatrix},\quad \underline{\epsilon}_2=\begin{bmatrix}\epsilon_x(2)\\ \epsilon_x(3)\end{bmatrix}.$$

However, now $\underline{h}^{(-1)}$ and $\underline{H}_{12}$ are 3×2, matrices $\underline{H}_{11}$ is a 3×3 matrix, $\underline{H}_{22}$ is a 2×2 matrix, and $\underline{h}^{(1)}$ and $\underline{H}_{21}$ are 2×3 matrices. The equation corresponding to (19) can be inverted to obtain (omitting the superscript eff)

$$e^{i\pi k_z}\underline{\epsilon}_1=-\underline{H}_{11}^{-1}(\underline{h}^{(-1)}\underline{\epsilon}_2+\underline{H}_{12}e^{i\pi k_z}\underline{\epsilon}_2)\ , \tag{D7}$$

and, from (20),

$$\underline{\epsilon}_2=-\underline{H}_{22}^{-1}(\underline{h}^{(1)}e^{i\pi k_z}\underline{\epsilon}_1+\underline{H}_{21}\underline{\epsilon}_1)\ . \tag{D8}$$

From these, we eliminate $\underline{\epsilon}_1$ to obtain, with $\underline{U}\equiv\underline{h}^{(1)}\underline{H}_{11}^{-1}\underline{H}_{12}$,

$$\begin{aligned}e^{i\pi k_z}(e^{i\pi k_z}\underline{\epsilon}_2)=&\underline{U}^{-1}[\underline{H}_{22}-(\underline{h}^{(1)}\underline{H}_{11}^{-1}\underline{h}^{(-1)}\\ &+\underline{H}_{21}\underline{H}_{11}^{-1}\underline{H}_{12})]e^{i\pi k_z}\underline{\epsilon}_2\\ &-\underline{U}^{-1}\underline{H}_{21}\underline{H}_{11}^{-1}\underline{h}^{(-1)}\underline{\epsilon}_2\\ \equiv&\underline{M}_{11}e^{i\pi k_z}\underline{\epsilon}_1+\underline{M}_{12}\underline{\epsilon}_2\ .\end{aligned}$$

Thus we have the eigenvalue equation

$$e^{i\pi k_z}\begin{bmatrix}e^{i\pi k_z}\epsilon_2\\ \underline{\epsilon}_2\end{bmatrix}=\begin{bmatrix}\underline{M}_{11} & \underline{M}_{12}\\ \underline{1}_{2\times2} & \underline{0}_{2\times2}\end{bmatrix}\begin{bmatrix}e^{i\pi k_z}\underline{\epsilon}_2\\ \underline{\epsilon}_2\end{bmatrix}, \tag{D9}$$

with four eigenvalues for $e^{i\pi k_z}$. Equations (D9) and (D7) then determine $\underline{\epsilon}_2$ and $\underline{\epsilon}_1$.

This result may seem somewhat astonishing at first, since we have five "independent" displacements for either B_1 or B_2 symmetry. To clarify the situation, we derive a different eigenvalue equation using the transfer-matrix theory.[30] We define "principal layer" and "superlayer" in the same way as in Ref. 30 for discussing electronic structures in the tight-binding approximation. In the present model, each superlayer contains two principal layers. The number of independent displacements in the two principal layers are denoted by μ and ν, respectively (see Fig. 17).

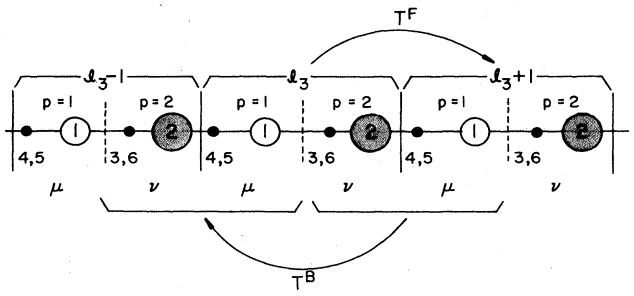

FIG. 17. Schematic diagram for the principal layers (labeled with $p=1,2$) and superlayers (labeled with l_3-1, l_3, and l_3+1); $\underline{T}^F$ and $\underline{T}^B$ denote the forward and backward transfer matrices which describe the propagation of transverse phonon modes. Only the transfer following the direction of the arrows is allowed.

Thus in the A_1 case, we have $\mu=\nu=3$. In the B_1 or B_2 case, we have $\mu=3$, $\nu=2$. Let $\underline{v}_1(l_3)$ and $\underline{v}_2(l_3)$ be $\mu\times1$ and $\nu\times1$ column vectors of the displacement in the two principal layers ($p=1,2$) of superlayer l_3. We can write the equations of motion corresponding to (19) and (20) as

$$\underline{h}^{(-1)}\underline{v}_2(l_3-1)+\underline{H}_{11}\underline{v}_1(l_3)+\underline{H}_{12}\underline{v}_2(l_3)=\underline{0}_{\mu\times1}\ , \tag{D10}$$

$$\underline{H}_{21}\underline{v}_1(l_3)+\underline{H}_{22}\underline{v}_2(l_3)+\underline{h}^{(1)}\underline{v}_1(l_3+1)=\underline{0}_{\nu\times1}\ , \tag{D11}$$

where $\underline{h}^{(-1)}$ and $\underline{H}_{12}$ are $\mu\times\nu$ matrices, $\underline{H}_{11}$ is a $\mu\times\mu$ matrix, $\underline{H}_{21}$ and $\underline{h}^{(1)}$ are $\nu\times\mu$ matrices, and $\underline{H}_{22}$ is a $\nu\times\nu$ matrix. When $\mu=\nu$, we can solve for either $\underline{v}_2(l_3-1)$ or $\underline{v}_2(l_3)$ from (D10), and also either $\underline{v}_1(l_3)$ or $\underline{v}_1(l_3+1)$ from (D11), and obtain the transfer matrices in the usual form, as in Ref. 30. When $\mu>\nu$, the situation becomes quite different. Given $\underline{v}_2(l_3-1)$ and $\underline{v}_1(l_3)$, the equation of motion (D10) overdetermines $\underline{v}_2(l_3)$, since there are μ equations for ν unknowns. Similarly, given $\underline{v}_1(l_3)$ and $\underline{v}_2(l_3)$, the equation of motion (D11) underdetermines $\underline{v}_1(l_3+1)$. This makes the argument in Ref. 30 inapplicable.

To obtain the transfer matrices in our case, we combine (D10) and (D11) to obtain

$$\begin{bmatrix}\underline{v}_2(l_3-1)\\ \underline{v}_1(l_3)\end{bmatrix}=\underline{T}^B\begin{bmatrix}\underline{v}_2(l_3)\\ \underline{v}_1(l_3+1)\end{bmatrix}, \tag{D12}$$

where

$$\underline{T}^B\equiv-\begin{bmatrix}\underline{0}_{\nu\times\nu} & \underline{H}_{21}\\ \underline{h}^{(-1)} & \underline{H}_{11}\end{bmatrix}^{-1}\begin{bmatrix}\underline{H}_{22} & \underline{h}^{(+1)}\\ \underline{H}_{12} & \underline{0}_{\mu\times\mu}\end{bmatrix} \tag{D13}$$

is referred to as the "backward transfer matrix." The first matrix on the right-hand side of (D13) is invertible, while the second is singular with $\mu-\nu$ zero eigenvalues. This is due to the existence of a $\mu\times\mu$ null matrix inside a $(\mu+\nu)\times(\mu+\nu)$ matrix with $\mu>\nu$.[31]

A "forward transfer matrix" $\underline{T}^F$ can be similarly defined by

$$\begin{bmatrix}\underline{v}_1(l_3+1)\\ \underline{v}_2(l_3+1)\end{bmatrix}=\underline{T}^F\begin{bmatrix}\underline{v}_1(l_3)\\ \underline{v}_2(l_3)\end{bmatrix}, \tag{D14}$$

where

$$\underline{T}^F\equiv-\begin{bmatrix}\underline{H}_{11} & \underline{H}_{12}\\ \underline{h}^{(1)} & \underline{0}_{\nu\times\nu}\end{bmatrix}^{-1}\begin{bmatrix}\underline{0}_{\mu\times\mu} & \underline{h}^{(-1)}\\ \underline{H}_{21} & \underline{H}_{22}\end{bmatrix}. \tag{D15}$$

A schematic diagram of the above relations is given in Fig. 17. We note that $\underline{T}^B$ and $\underline{T}^F$ are not simple inverses of each other. In fact, both $\underline{T}^B$ and $\underline{T}^F$ are singular matrices, with $\mu-\nu$ zero eigenvalues. The zero eigenvalues in $e^{ik_z\pi}$ (for $\underline{T}^F$) and $e^{-ik_z\pi}$ (for $\underline{T}^B$) correspond to complex k_z solutions with $k_i\to\infty$ and $-\infty$, respectively. These solutions are nonphysical and, hence, are not needed in the calculation of heterostructure phonon properties.

We now discuss the extension of the superlattice phonon calculation with $\vec{k}_{||}=\vec{0}$. For the A_1 case the $\vec{k}_{||}\neq\vec{0}$

method needs only trivial modifications, as described in the text. For the B_2 case we find that expression (33) does not apply to the displacements of the first layer in each material (i.e., $\underline{v}_1^{(\sigma)}$, $\sigma=A,B$) for all L, as shown by a consideration of the properties of the forward and backward transfer matrices. In other words, the basis $\phi_j(\sigma)$ defined in (38) is not complete for the expression of the displacement eigenvector of the superlattice. We must also include the "old" basis vectors at $l_3=1$, $\psi_\alpha^{(\sigma)}(1)$ with $\kappa,\alpha=1,x,4,x,4,z$. The equations of motion (34) and (35) are still valid for the B_2 case. However, we need additional equations to relate $\underline{v}_1^{(\sigma)}(1)$ to $\underline{C}^{(A)}$ and $\underline{C}^{(B)}$. We use the equations of motion corresponding to (D11) for $L=0$, $l_3=1$, $\sigma=A,B$, and (33)–(35) to obtain a 14×14 matrix equation,

$$\begin{bmatrix} \underline{Y}_{11} & \underline{0} & \underline{Y}_{13} & \underline{Y}_{14} \\ \underline{0} & \underline{Y}_{22} & \underline{Y}_{23} & \underline{Y}_{24} \\ \underline{Y}_{31} & \underline{Y}_{32} & \underline{Y}_{33} & \underline{0} \\ \underline{Y}_{41} & \underline{Y}_{42} & \underline{0} & \underline{Y}_{44} \end{bmatrix} \begin{bmatrix} \underline{C}^{(A)} \\ \underline{C}^{(B)} \\ \underline{v}_1^{(A)}(1) \\ \underline{v}_1^{(B)}(1) \end{bmatrix} = \underline{0}\,, \tag{D16}$$

where

$$\underline{Y}_{11}=\begin{bmatrix} \underline{H}_{22}^{(A)}\underline{F}_2^{(A)}(1)+\underline{h}_A^{(1)}\underline{F}_1^{(A)}(2) \\ \underline{H}_{21}^{(A)}\underline{F}_1^{(A)}(\underline{n}_A)+\underline{\tilde{H}}_{22}^{(A)}\underline{F}_2^{(A)}(n_A) \end{bmatrix},$$

$$\underline{Y}_{13}=\begin{bmatrix} \underline{H}_{21}^{(A)} \\ \underline{0} \end{bmatrix},\quad \underline{Y}_{14}=\begin{bmatrix} \underline{0} \\ \underline{h}_{AB}^{(1)} \end{bmatrix},$$

$$\underline{Y}_{23}=\begin{bmatrix} \underline{0} \\ e^{iq\pi}\underline{h}_{BA}^{(1)} \end{bmatrix},\quad \underline{Y}_{24}=\begin{bmatrix} \underline{0} \\ \underline{H}_{21}^{(B)} \end{bmatrix},$$

$$\underline{Y}_{31}=\underline{H}_{12}^{(A)}\underline{F}_2^{(A)}(1),\quad \underline{Y}_{32}=\underline{h}_{AB}^{(-1)}\underline{F}_2^{(B)}(n_B)e^{-iq\pi},$$

$$\underline{Y}_{33}=\underline{\tilde{H}}_{11}^{(A)},$$

$$\underline{Y}_{41}=\underline{h}_{BA}^{(-1)}\underline{F}_2^{(A)}(n_A),\quad \underline{Y}_{42}=\underline{H}_{12}^{(B)}\underline{F}_2^{(B)}(1),$$

$$\underline{Y}_{44}=\underline{\tilde{H}}_{11}^{(B)},$$

and $\underline{Y}_{22}$ is in the same form as $\underline{Y}_{11}$ with the index A replaced by B.

As in the previous case, we can multiply the matrix $\underline{Y}$ in (D16) by a matrix $\underline{G}^\dagger$ to obtain a Hermitian matrix, $\underline{X}$ where

$$\underline{G}^\dagger=\begin{bmatrix} \underline{G}_A^\dagger & \underline{0} & \underline{0} & \underline{0} \\ \underline{0} & \underline{G}_B^\dagger & \underline{0} & \underline{0} \\ \underline{0} & \underline{0} & \underline{\mathbb{1}}_{3\times3} & \underline{0} \\ \underline{0} & \underline{0} & \underline{0} & \underline{\mathbb{1}}_{3\times3} \end{bmatrix},$$

with

$$\underline{G}_A=\begin{bmatrix} \underline{F}_2^{(A)}(1) \\ \underline{F}_2^{(A)}(n_A) \end{bmatrix},\quad \underline{G}_B=\begin{bmatrix} \underline{F}_2^{(B)}(1) \\ \underline{F}_2^{(B)}(n_B) \end{bmatrix},$$

and $\underline{\mathbb{1}}_{3\times3}$ is a three-dimensional identity matrix. We can then proceed in the same way as in the previous case to find the solutions.

[1] J. N. Schulman and T. C. McGill, in *Synthetic Modulated Structure Materials,* edited by L. L. Chung and B. C. Giessen (Academic, New York, in press).

[2] S. M. Rytov, Akust. Zh. **2**, 71 (1956) [Sov. Phys.—Acoust. **2**, 68 (1956)].

[3] A. S. Barker, J. L. Merz, and A. C. Gossard, Phys. Rev. B **17**, 3181 (1978).

[4] R. Merlin, C. Colvard, M. V. Klein, H. Morkoç, A. Y. Cho, and A. C. Gossard, Appl. Phys. Lett. **36**, 43 (1980).

[5] A. A. Maradudin, E. W. Montroll, G. H. Wiess, and I. P. Ipatova, *Theory of Lattice Dynamics in the Harmonic Approximation,* 2nd ed. (Academic, New York, 1971).

[6] V. Keine, Proc. Phys. Soc. London **81**, 300 (1963).

[7] J. N. Schulman and Y. C. Chang, Phys. Rev. B **24**, 4445 (1981).

[8] Y. C. Chang, Phys. Rev. B **25**, 605 (1982); Y. C. Chang and J. N. Schulman, *ibid.* **25**, 3975 (1982).

[9] W. Weber, Phys. Rev. Lett. **33**, 371 (1974).

[10] K. C. Rustagi and W. Weber, Solid State Commun. **18**, 673 (1976).

[11] W. Weber, Phys. Rev. B **15**, 4789 (1977).

[12] R. M. Martin, Phys. Rev. **186**, 871 (1969).

[13] W. Cochran, Proc. R. Soc. London, Ser. A **253**, 260 (1959).

[14] P. N. Keating, Phys. Rev. **145**, 637 (1966).

[15] P. H. Borcherds, G. F. Alfrey, D. H. Samderson, and A. D. B. Woods, J. Phys. C **8**, 2022 (1975).

[16] M. Vandevyyer and P. Plumelle, J. Phys. Chem. Solids **38**, 765 (1977).

[17] P. H. Borcherds and K. Kunc, J. Phys. C **11**, 4145 (1978).

[18] D. N. Talwar and B. K. Agrawal, Phys. Status Solidi B **63**, 441 (1974).

[19] The experimental data were compiled by H. Bliz and W. Kress, in *Phonon Dispersion Relations in Insulators,* Vol. 10 of *Springer Series in Solid State Sciences,* edited by M. Cardona, P. Fulde, and H. J. Queisser (Springer, New York, 1979).

[20] A. Onton and R. J. Chicotka, Phys. Rev. B **10**, 591 (1974).

[21] It is noted that the present phonon model in the zeroth-order approximation is very analogous to a nearest-neighbor tight-binding model for electronic structures with nine orbitals per atom, which correspond to the nine independent displacements associated with a cation or anion as defined in (18).

[22] E. I. Blount, in *Solid State Physics,* edited by F. Seitz and D. Turnbull (Academic, New York, 1962), Vol. 13.

[23] C. Colvard, R. Merlin, M. V. Klein, and A. C. Gossard, Phys. Rev. Lett. **45**, 298 (1980).

[24] M. V. Klein, C. Colvard, R. Fisher, and H. Morkoç, in Proceedings of the International Conference on the Dynamics of Interfaces, Lille, France, 1983 (unpublished).

[25] C. Colvard, Ph.D. thesis, University of Illinois at Urbana–Champaign, 1983.

[26] There is a misprint in Ref. 11.

[27] S. Y. Tong and A. A. Maradudin, Phys. Rev. **181**, 1318 (1969).

[28] I. S. Gradshteyn and I. M. Ryzhik, *Tables of Integrals, Series and Products* (Academic, New York, 1980).

[29] A. P. Cracknell, *Applied Group Theory* (Pergamon, New York, 1968).

[30] D. H. Lee and J. D. Joannopoulos, Phys. Rev. B **23**, 4988

(1981).

[31]Any $(\mu+\nu)\times(\mu+\nu)$ matrix with a $\mu\times\mu$ null matrix entry can be rearranged in the following form:

$$\begin{bmatrix} \underline{A} & \underline{B} \\ \underline{0}_{\nu\times\mu} & \underline{C} \end{bmatrix}, \quad \underline{A} = \begin{bmatrix} \underline{D} & \underline{E} \\ \underline{0}_{(\mu-\nu)\times\nu} & \underline{0}_{(\mu-\nu)\times(\mu-\nu)} \end{bmatrix},$$

where $\underline{D}$ is a $\nu\times\nu$ matrix, $\underline{E}$ is a $\nu\times(\mu-\nu)$ matrix, $\underline{B}$ is a $\mu\times\nu$, and $\underline{C}$ is a $\nu\times\nu$ matrix. It is obvious that the determinant of the matrix is $\det(\underline{D})\det(\underline{C})(\mu-\nu)$ zeros.